Isostable Reduction of Oscillators with Piecewise Smooth Dynamics and Complex Floquet Multipliers

Dan Wilson
Department of Electrical Engineering and Computer Science,
University of Tennessee, Knoxville, TN 37996, USA

Phase-amplitude reduction is a widely applied technique in the study of limit cycle oscillators with the ability to represent a complicated and high-dimensional dynamical system in a more analytically tractable coordinate system. Recent work has focused on the use of isostable coordinates, which characterize the transient decay of solutions towards a periodic orbit, and can ultimately be used to increase the accuracy of these reduced models. The breadth of systems to which this phase-amplitude reduction strategy can be applied, however, is still rather limited. In this work, the theory of phase-amplitude reduction using isostable coordinates is further developed to accommodate a broader set of dynamical systems. In the first part, limit cycles of piecewise smooth dynamical systems are considered and strategies are developed to compute the associated reduced equations. In the second part, the notion of isostable coordinates for complex-valued Floquet multipliers is introduced resulting in one phase-like coordinate and one amplitude-like coordinate for each pair of complex conjugate Floquet multipliers. Examples are given with relevance to piecewise smooth representations of excitable cardiomyocytes and the relationship between the reduced coordinate system and the emergence of cardiac alternans is discussed. Also, phase-amplitude reduction is implemented for a chaotic, externally forced pendulum with complex Floquet multipliers and a resulting control strategy for the stabilization of its periodic solution is investigated.

I. INTRODUCTION

Periodic oscillations are extensively studied in the nonlinear sciences with a wide variety of applications including brain rhythms [1], [2], circadian oscillations, [3], [4], and cardiac function [5], [6]. While most of these aforementioned dynamical systems are modeled with high-dimensional, nonlinear differential equations, analysis can be made more tractable through the use of phase reduction [3], [2], [7]. To illustrate the notion of phase reduction, consider an autonomous vector field of the form

$$\dot{\mathbf{x}} = \mathbf{F}(\mathbf{x}) + \mathbf{u}(t), \tag{1}$$

where $\mathbf{x} \in \mathbb{R}^n$ is the state of the system, $\mathbf{F}$ represents the unperturbed dynamics, and $\mathbf{u}(t)$ is an $\mathcal{O}(\epsilon)$ exogenous perturbation where $0 < \epsilon \ll 1$. From this point forward it will be assumed that Eq. (1) admits a stable limit cycle solution $\mathbf{x}^\gamma(t)$ with period T in the absence of perturbation. Because this orbit is topologically equivalent to a circle, the notion of the "phase" of oscillation $\mathbf{x} \mapsto \theta \in \mathbb{S}^1$ has been employed for many decades as a method of model reduction [3], [7], [8]. Changing to phase coordinates via the chain rule yields

$$\begin{aligned}
\frac{d\theta}{dt} &= \frac{\partial \theta}{\partial \mathbf{x}} \cdot \frac{d\mathbf{x}}{dt}, \\
&= \frac{\partial \theta}{\partial \mathbf{x}} \cdot (\mathbf{F}(\mathbf{x}) + \mathbf{u}(t)),
\end{aligned} \tag{2}$$

where "$\cdot$" indicates the dot product. The exact definition of phase differs in various contexts, but one of the more commonly used definitions relies on the notion of an asymptotic phase through the calculation of isochrons [3], [9]. Specifically, in the absence of external perturbation (i.e., when $\mathbf{u}(t) = 0$), for a given location $\mathbf{x}^\delta$ in the basin of attraction of the limit cycle $\mathcal{B}(\gamma)$ the associated asymptotic phase can be defined as the unique $\theta(\mathbf{x}^\delta) \in [0, 2\pi)$ that satisfies

$$\lim_{t \to \infty} \left| \phi(t, \mathbf{x}^\delta) - \phi\left(t + \frac{T}{2\pi}\theta(\mathbf{x}^\delta), \mathbf{x}^\gamma(0)\right) \right| = 0, \tag{3}$$

where ϕ is the unperturbed flow. Level sets of the phase as defined in Eq. (3) are often referred to as isochrons [3], [9]. Using this definition, one can verify that when $\mathbf{u}(t) = 0$, $d\theta/dt = 2\pi/T \equiv \omega$ which implies that $\frac{\partial \theta}{\partial \mathbf{x}} \cdot \mathbf{F}(\mathbf{x}) = \omega$ so that Eq. (2) can be rewritten simply in terms of phase coordinates [2], [7],

$$\frac{d\theta}{dt} = \omega + \mathbf{Z}(\theta) \cdot \mathbf{u}(t), \tag{4}$$

where $\mathbf{Z}(\theta)$ denotes the gradient of the phase evaluated on the periodic orbit and is often called the infinitesimal phase response curve (PRC).

Equation (4) is valid provided the state remains close to the stable limit cycle. Typically, this requires the magnitude of the allowable perturbations to be small relative to the magnitude of the Floquet multipliers [10], which characterize the rate of convergence to the limit cycle. However, in many applications, larger perturbations are required, necessitating the use of phase-amplitude coordinate systems that incorporate the dynamics in directions transverse to the limit cycle of Eq. (1). For instance, [11] and [12] use moving orthonormal coordinate systems to study such behavior. Additionally, in experimental applications where noise makes asymptotic behavior difficult to infer, readily measurable characteristics (such as a neural action potential in a tonically firing neuron) have been used to define phase. In many cases this definition requires the use of residual or higher order PRCs [13] [14], [15], that are used to model memory in a system, i.e., to quantify how perturbations from previous cycles affect the spike time on the current cycle. Additionally, building upon behavior of linear, time-varying periodic systems described by Floquet theory [10], the authors of [16], [17], [18] investigate the behavior of a coordinate system comprised of the asymptotic phase from Eq. (3) and $n-1$ additional coordinates which decay exponentially to zero in the absence of perturbations.

This work will focus on the reduction strategy based on Floquet theory as used in [16], [17], [18]. In prior work [17] uses the notion of isostable coordinates which represent level sets of initial conditions that approach the periodic orbit together in a well defined sense. By comparing the decay towards the periodic orbit to the exponentially decaying basis of eigenvectors set forth by Floquet theory [10], isostable coordinates ψ_j for $1 \le j \le n-1$ can be defined. In [19], it was shown that this isostable coordinate system could be used to derive a second-order accurate phase-amplitude reduction of the form:

$$\dot{\theta} = \omega + \mathbf{Z}(\theta) \cdot \mathbf{u}(t) + \sum_{k=1}^{n-1} \left[\mathbf{B}^k(\theta) \psi_k \right] \cdot \mathbf{u}(t),$$

$$\dot{\psi}_j = \kappa_j \psi_j + \mathbf{I}_j(\theta) \cdot \mathbf{u}(t) + \sum_{k=1}^{n-1} \left[\mathbf{C}_j^k(\theta) \psi_k \right] \cdot \mathbf{u}(t),$$

$$j = 1, \ldots, n-1. \tag{5}$$

Here, ψ_j denotes an isostable coordinate associated with one of the non-unity Floquet multipliers of the periodic orbit with Floquet exponent κ_j, $\mathbf{I}_j(\theta) \equiv \frac{\partial \psi_j}{\partial \mathbf{x}}$ denotes the gradient of the isostable coordinate evaluated at $\mathbf{x}^\gamma(\theta)$ and will be referred to as the infinitesimal isostable response curve (IRC), $\mathbf{B}^k(\theta) \equiv \frac{\partial^2 \theta}{\partial \mathbf{x}^2} \left(\frac{\partial \mathbf{x}}{\partial \psi_k} \right)$, and $\mathbf{C}_j^k \equiv \frac{\partial^2 \psi_j}{\partial \mathbf{x}^2} \left(\frac{\partial \mathbf{x}}{\partial \psi_k} \right)$ provide nonlinear corrections as the system is perturbed from its periodic orbit. All of the functions above are evaluated on the periodic orbit at phase θ. Equation (5) is identical to Equation (47) from [19] (used in prior work). For systems with higher dimension, many Floquet multipliers may be close to zero yielding negative values κ_j which are large in magnitude. In this case, it is generally assumed that the isostable coordinates associated with these Floquet multipliers are always zero (c.f. [19], [20]), leading to a reduction in dimension as compared to Eq. (1). Higher order corrections to the phase reduced dynamics have been studied in other contexts. For instance [8] uses such an expansion to obtain the frequency change of an oscillator in response to parameter perturbations. Additionally, [21] and [22] use higher order corrections to characterize neural spiking statistics in response to ion channel fluctuations wherein the notion of radial susceptibilities is analogous to the IRCs considered in this work.

The transformation of the dynamical system from Eq. (1) to the reduction from Eqs. (5) has been shown to be useful in contexts where the standard phase reduction from Eq. (4) is inadequate, i.e., when large magnitude perturbations are applied [19], [20]. However, the methodology described in both [19] and [20] requires all Floquet exponents to be real and requires that $\mathbf{F}(\mathbf{x})$ is sufficiently smooth in order to compute the reduced functions $\mathbf{Z}(\theta)$, $\mathbf{B}^k(\theta)$, $\mathbf{I}(\theta)$ and $\mathbf{C}_j^k(\theta)$. These limitations exclude many categories of dynamical systems. For instance, complex Floquet multipliers can often be observed in systems with external forcing such as the Brusselator [23], circadian models such as [24] in response to the periodic application of

light, and the periodically forced pendulum [25]. The emergence of complex Floquet multipliers replicates the quasiperiodicity associated with the discrepancy between a system's natural frequency in the absence of perturbation and the frequency of the external forcing. Furthermore, the aforementioned violation of sufficiently smooth flow is a quality of dynamical systems which display a sudden change in behavior. Practical examples can be found in equations that model repolarization dynamics in cardiac action potentials [26], [27], switching between day and night in circadian oscillators [28], [29], integrate-and-fire neurons [30], and mechanical oscillators with Coulomb friction [31]. Particular attention in this work will be given to a low dimensional model of single cardiomyocytes given in [26] which is designed to replicate the qualitative behavior of much larger and more complicated models. In exchange for lower dimensionality, however, the model equations from [31] are nonsmooth requiring additional considerations when computing the terms of the phase-amplitude reduction.

In this paper, strategies are developed to make phase-amplitude reduction based on isostable coordinates as given in Eqs. (5) applicable to piecewise smooth dynamical systems and limit cycles with complex-valued Floquet multipliers. In the case where piecewise smooth dynamical systems are of interest, it will be necessary to derive jump conditions which determine how the PRC, IRC, and other equations from the reduced Eqs. (5) change across boundaries where the vector field $\mathbf{F}(\mathbf{x})$ is discontinuous. In cases where a Floquet multiplier is complex, a new definition of isostable coordinates will be used resulting in a reduced set of equations that is different than Eqs. (5). The organization of this paper is as follows: Section II gives necessary background information on isostable coordinates for representing dynamical behavior in directions transverse to a periodic orbit. Most of Section II constitutes a review of theory formulated in [19] and [20], however, Section II B provides an improved approach for the computation of $\mathbf{B}^k(\theta)$ and $\mathbf{C}_j^k(\theta)$ from Eq. (5). Section III derives a strategy for calculating the PRC, IRC and other terms of Eqs. (5) for piecewise smooth dynamical systems, and applies this strategy to investigate the behavior of a cardiac model [26] in a reduced framework. Section IV defines isostable coordinates for use when Floquet multipliers are complex, uses it to develop a reduced set of equations similar to Eqs. (5) and applies this strategy to control a chaotic model of a forced pendulum. Section V gives concluding remarks.

II. BACKGROUND ON ISOSTABLE COORDINATES AND ISOSTABLE REDUCTION

This section provides important background on isostable coordinates used in the derivation of the second order phase-amplitude reduction from Eq. (5). The analysis starting with Eq. (6) and ending with Eq. (16) also appears in [19] and is summarized here for convenience. To begin, consider a limit cycle solution $\mathbf{x}^\gamma(t)$ of the dynamical system from Eq. (1). In order to define isostable coordinates for this system the transient behavior of solutions near the periodic orbit will be considered. Let Γ_0 correspond to the $\theta(\mathbf{x}) = 0$ isochron defined according to Eq. (3). By definition, the return time from Γ_0 back to Γ_0 is T allowing for the definition of a Poincaré map:

$$P : \Gamma_0 \to \Gamma_0;$$
$$\mathbf{x} \to \phi(T, \mathbf{x}), \tag{6}$$

recalling that ϕ is the unperturbed flow. This map has a fixed point $\mathbf{x}_0$ corresponding to the intersection of $\mathbf{x}^\gamma(t)$ and the $\theta = 0$ isochron. In a neighborhood of $\mathbf{x}_0$, the Poincaré map can be approximated through linearization as

$$\phi(T, \mathbf{x}) = \mathbf{x}_0 + J_p(\mathbf{x} - \mathbf{x}_0), \tag{7}$$

where J_p is the Jacobian of ϕ evaluated at $\mathbf{x}_0$. By assuming that J_p is diagonalizable, one can define right and left eigenvectors $\mathbf{v}_k$ and $\mathbf{w}_k^T$, respectively, associated with the Floquet multipliers λ_k for $k = 1 \ldots N$ which are related to the Floquet exponents, κ_k, by the relation $\kappa_k = \log(\lambda_k)/T$.

For all non-zero Floquet exponents, one can define isostable coordinates as in [19] (c.f. [17]) according to

$$\psi_k(\mathbf{x}) = \lim_{j \to \infty} \left[\mathbf{w}_k^T (\phi(t_\Gamma^j, \mathbf{x}) - \mathbf{x}_0) \exp(-\kappa_k t_\Gamma^j) \right], \tag{8}$$

where t_Γ^j denotes the jth return time to Γ_0 under the flow. When λ_k is real and positive, κ_k is real in the above definition of isostable coordinates. The definition from Eq. (8) is only valid for stable periodic

orbits where the real component of all non-zero Floquet exponents is negative. Intuitively, when using this definition to evaluate the isostable coordinate of a particular state an exponentially growing function on the right is multiplied by a function of the state that shrinks at the same rate; in the limit as time approaches infinity, the product approaches a number which gives the isostable coordinate. Note that when λ_k is negative or imaginary (resulting in a complex value of κ_k) Eq. (8) will still yield a scalar isostable coordinate. Additionally, as one can verify, when $\mathbf{u}(t) = 0$, $d\psi_k/dt = \kappa_k \psi_k$. In Eq. (8), isostable coordinates are defined according to the infinite time convergence to the limit cycle solution. This is different than the isostable definition used in [17] where a finite time calculation was employed to study the perturbed behavior of unstable periodic orbits.

In order to derive the isostable reduction from Eqs. (5), one can expand the gradients of the phase and isostable coordinates as

$$
\begin{aligned}
\left.\frac{\partial \theta}{\partial \mathbf{x}}\right|_{\mathbf{x}^\gamma(\theta)+\Delta\mathbf{x}} &= \left.\frac{\partial \theta}{\partial \mathbf{x}}\right|_{\mathbf{x}^\gamma(\theta)} + \left.\frac{\partial^2 \theta}{\partial \mathbf{x}^2}\right|_{\mathbf{x}^\gamma(\theta)} \Delta\mathbf{x} + \mathcal{O}(|\Delta\mathbf{x}|^2), \\
&= \mathbf{Z}(\theta) + H_{\theta,\mathbf{x}^\gamma(\theta)}\Delta\mathbf{x} + \mathcal{O}(|\Delta\mathbf{x}|^2),
\end{aligned}
\tag{9}
$$

$$
\begin{aligned}
\left.\frac{\partial \psi_k}{\partial \mathbf{x}}\right|_{\mathbf{x}^\gamma(\theta)+\Delta\mathbf{x}} &= \left.\frac{\partial \psi_k}{\partial \mathbf{x}}\right|_{\mathbf{x}^\gamma(\theta)} + \left.\frac{\partial^2 \psi_k}{\partial \mathbf{x}^2}\right|_{\mathbf{x}^\gamma(\theta)} \Delta\mathbf{x} + \mathcal{O}(|\Delta\mathbf{x}|^2), \\
&= \mathbf{I}_k(\theta) + H_{\psi_k,\mathbf{x}^\gamma(\theta)}\Delta\mathbf{x} + \mathcal{O}(|\Delta\mathbf{x}|^2),
\end{aligned}
\tag{10}
$$

$$
k = 1, \ldots, n-1.
$$

Here, $H_{\theta,\mathbf{x}^\gamma(\theta)}$ and $H_{\psi_k,\mathbf{x}^\gamma(\theta)}$ represent the Hessian of θ and ψ_k evaluated at $\mathbf{x}^\gamma(\theta)$. For locations near the periodic orbit, Floquet theory [10], [32] allows us write perturbations to $\mathbf{x}^\gamma(\theta)$ as a set of exponentially decaying modes. To do so, let $\mathbf{x}_\epsilon(t) = \mathbf{x}^\gamma(t) + \Delta\mathbf{x}(t)$ be a solution to Eq. (1), where $\Delta x(t)$ is an order ϵ term. When $\mathbf{u}(t) = 0$, one can can write

$$
\frac{d\Delta\mathbf{x}}{dt} = DF(\mathbf{x}^\gamma(t))\Delta\mathbf{x}(t) + \mathcal{O}(|\Delta\mathbf{x}|^2),
\tag{11}
$$

where $DF(\mathbf{x}^\gamma(t))$ is the Jacobian evaluated at $\mathbf{x}^\gamma(t)$. From Floquet theory, [10], [32], solutions of Eq. (11) can be written as

$$
\Delta\mathbf{x}(t) = \sum_{k=1}^{n} c_k \exp(\kappa_k t)\mathbf{p}_k(\theta(t)),
\tag{12}
$$

where c_k are constants determined by initial conditions, κ_k are Floquet exponents, and $\mathbf{p}_k(\theta(t))$ are T-periodic functions that can be approximated according to

$$
\begin{aligned}
\mathbf{p}_k(\theta) &= \mathbf{p}_k^t(t\omega) \\
\mathbf{p}_k^t(t) &\equiv \frac{[\phi(t, \epsilon\mathbf{v}_k + \mathbf{x}_0) - \phi(t, \mathbf{x}_0)]\exp(-\kappa_k t)}{\epsilon}
\end{aligned}
\tag{13}
$$

for $0 < \epsilon \ll 1$. As shown in [19], $\Delta\mathbf{x}$ from Eq. (9) can be written in terms of phase and isostable coordinates as

$$
\Delta\mathbf{x}(\theta, \psi_1, \ldots, \psi_{n-1}) = \sum_{k=1}^{n-1} (\psi_k \mathbf{p}_k(\theta)).
\tag{14}
$$

Equation (14) and other relationships between the state and the dynamics in directions transverse to a stable periodic orbit are particularly important in the development of second order accurate reduction strategies. These issues have been explored previously and the interested reader is referred to [8], [22], [21] for a detailed discussion. Substituting Eq. (14) into Eq. (9), one can show that the terms from the second order corrections from Eqs. (5) are given by

$$
\mathbf{B}^k(\theta) = H_{\theta,\mathbf{x}^\gamma(\theta)}\mathbf{p}_k(\theta),
\tag{15}
$$

$$
\mathbf{C}_j^k(\theta) = H_{\psi_j,\mathbf{x}^\gamma(\theta)}\mathbf{p}_k(\theta).
\tag{16}
$$

A.   Previously Developed Strategies for the Calculation of the Phase-Amplitude Equations

Various strategies for the calculation of the terms from the second order reduction as given in Eqs. (5) have been developed. It is well documented that the functions $\nabla_{\mathbf{x}^\gamma(t)}\theta \equiv \mathbf{Z}(\theta)$ and $\nabla_{\mathbf{x}^\gamma(t)}\psi_k \equiv \mathbf{I}_k(\theta)$ can be calculated as the periodic solution to the adjoint equation [8], [33], [17]

$$\frac{d\nabla_{\mathbf{x}^\gamma(t)}\theta}{dt} = -DF(\mathbf{x}^\gamma(t))^T\nabla_{\mathbf{x}(t)}\theta, \tag{17}$$

$$\frac{d\nabla_{\mathbf{x}^\gamma(t)}\psi_k}{dt} = \left(\kappa_k I - DF(\mathbf{x}^\gamma(t))^T\right)\nabla_{\mathbf{x}(t)}\psi_k, \tag{18}$$

where $DF(\mathbf{x}^\gamma(t))$ is the Jacobian of $\mathbf{F}$ evaluated at $\mathbf{x}^\gamma(t)$ and I denotes the identity matrix. Here, Eq. (17) is normalized so that $\mathbf{F}(\mathbf{x}(\theta))\cdot\nabla_{\mathbf{x}(t)}\theta = \omega$ and each solution of Eq. (18) is normalized so that $\mathbf{v}_k\cdot\nabla_{\mathbf{x}(t)}\psi_k = 1$ when evaluated at $\theta = 0$. Because $\mathbf{u}(t)$ is generally assumed to be an $\mathcal{O}(\epsilon)$ term, both $\mathbf{Z}(\theta)\cdot\mathbf{u}(t)$ and $\mathbf{I}_k(\theta)\cdot\mathbf{u}(t)$ represent $\mathcal{O}(\epsilon)$ terms in Eqs. (5).

One strategy for computation of $\mathbf{B}^k(\theta)$ and $\mathbf{C}_j^k(\theta)$ (which characterize the $\mathcal{O}(\epsilon^2)$ terms in Eqs. (5)) is to directly calculate $H_{\theta,\mathbf{x}^\gamma(\theta)}$ and $H_{\psi_j,\mathbf{x}^\gamma(\theta)}$. As shown in [19], these Hessians can be calculated as periodic solutions to the following equations

$$\frac{dH_{\theta,\mathbf{x}^\gamma(t)}}{dt} = -\sum_{k=1}^n\left[Z^k(\mathbf{x}^\gamma(t))H_{k,\mathbf{x}^\gamma(t)}\right]$$
$$- DF^T(\mathbf{x}^\gamma(t))H_{\theta,\mathbf{x}^\gamma(t)} - H_{\theta,\mathbf{x}^\gamma(t)}DF(\mathbf{x}^\gamma(t)), \tag{19}$$

$$\frac{dH_{\psi_j,\mathbf{x}^\gamma(t)}}{dt} = \kappa_j H_{\psi_j,\mathbf{x}^\gamma(t)} - \sum_{k=1}^n\left[I_j^k(\mathbf{x}^\gamma(t))H_{k,\mathbf{x}^\gamma(t)}\right]$$
$$- DF^T(\mathbf{x}^\gamma(t))H_{\psi_j,\mathbf{x}^\gamma(t)} - H_{\psi_j,\mathbf{x}^\gamma(t)}DF(\mathbf{x}^\gamma(t)), \tag{20}$$

where $Z^k(\mathbf{x}^\gamma(t)) \equiv \partial\theta/\partial x_i$ and $I_j^k(\mathbf{x}^\gamma(t)) \equiv \partial\psi_j/\partial x_i$ evaluated on the periodic orbit (i.e., the kth components of the PRC and IRC) and $H_{k,\mathbf{x}^\gamma(t)}$ is the Hessian matrix of the kth component of $\mathbf{F}$ evaluated at $\mathbf{x}^\gamma(t)$ (i.e., $H_{k,\mathbf{x}^\gamma(t)} \equiv [D^2 F_k]\big|_{\mathbf{x}^\gamma(t)}$). Note that equations (19) and (20) are identical to Eqs. (19) and (44) from [19]. Equations (19) and (20) must be normalized according to the relations

$$-DF(\mathbf{x}^\gamma(t))^T\mathbf{Z}(\theta(t)) = H_{\theta,\mathbf{x}^\gamma(t)}\mathbf{F}(\mathbf{x}^\gamma(t)) \tag{21}$$

and

$$(\kappa_j I - DF(\mathbf{x}^\gamma(t))^T)\mathbf{I}_j(\theta(t)) = H_{\psi_j,\mathbf{x}^\gamma(t)}\mathbf{F}(\mathbf{x}^\gamma(t)), \tag{22}$$

respectively.

The size of matrices $H_{\theta_j,\mathbf{x}^\gamma(t)}$ and $H_{\psi_j,\mathbf{x}^\gamma(t)}$ grow in proportion to $n \times n$ which presents a challenge for their computation for high dimensional systems. For this reason, a different strategy is proposed in [20] where each of the terms $\mathbf{B}^k(\theta)$ are calculated individually. Because each $\mathbf{B}^k(\theta) \in \mathbb{R}^n$, this reduces the size of the equation which must be calculated. Additionally, because some isostable coordinates associated with Floquet multipliers near zero are neglected, only a subset of the $\mathbf{B}^k(\theta)$ functions must be calculated.

As illustrated in [20], the term $\mathbf{B}^k(\theta)$ can be calculated by first defining $\mathbf{x}_{\epsilon,k}(t) \equiv \phi(t,\mathbf{x}_0 + \epsilon\mathbf{v}_k)$, i.e., the unperturbed flow of (1) for an initial condition corresponding to $\theta = 0$, $\psi_k = \epsilon$, and $\psi_j = 0$ for $j \neq k$ where $|\epsilon| \ll 1$. With this definition, one can show that

$$\mathbf{B}^k(t) = \frac{\exp(-\kappa_k t)}{\epsilon}\left(\frac{\partial\theta}{\partial\mathbf{x}}\bigg|_{\mathbf{x}_{\epsilon,k}(t)} - \frac{\partial\theta}{\partial\mathbf{x}}\bigg|_{\mathbf{x}^\gamma(t)}\right), \tag{23}$$

where, $\partial\theta/\partial\mathbf{x}\big|_{\mathbf{x}_{\epsilon,k}(t)} \equiv \nabla_{\mathbf{x}_{\epsilon,k}(t)}\theta$ is the solution of the adjoint equation as given in Eq. (17)

$$\frac{d\nabla_{\mathbf{x}_{\epsilon,k}(t)}\theta}{dt} = -J(\mathbf{x}_{\epsilon,k}(t))^T\nabla_{\mathbf{x}_{\epsilon,k}(t)}\theta, \tag{24}$$

subject to the boundary condition

$$\left.\frac{\partial\theta}{\partial\mathbf{x}}\right|_{\mathbf{x}_{\epsilon,k}(T)} - \left.\frac{\partial\theta}{\partial\mathbf{x}}\right|_{\mathbf{x}^{\gamma}(T)} = \exp(\kappa_k T)\left(\left.\frac{\partial\theta}{\partial\mathbf{x}}\right|_{\mathbf{x}_{\epsilon,k}(0)} - \left.\frac{\partial\theta}{\partial\mathbf{x}}\right|_{\mathbf{x}^{\gamma}(0)}\right). \tag{25}$$

While the calculation of $\mathbf{B}^k(\theta)$ according to Eq. (23) is computationally less demanding than doing so by first calculating $H_{\theta,\mathbf{x}^{\gamma}}(\theta)$ using Eq. (19), practical implementation requires a choice of ϵ which is small enough so that the perturbed behavior is well approximated by Eq. (14), but not so small that the numerical algorithm induces errors due to limits in floating point precision. A good choice of ϵ is not known *a priori*, and in some cases this can make it difficult to find $\mathbf{B}^k(\theta)$ using Eq. (23).

B.   An Alternative Strategy for Calculation of Second Order Terms

Considering the limitations discussed above, here a strategy is developed for computing the second order terms $\mathbf{B}^k(\theta)$ and $\mathbf{C}_j^k(\theta)$ from Eqs. (5) with computational effort proportional to n. Additionally, this strategy does not suffer from the same numerical limitations as the strategy as given in Eq. (23).

To begin, consider the relation from Eq. (19) multiplied on the right by any small perturbation from the limit cycle $\Delta\mathbf{x}(t)$

$$\frac{dH_{\theta,\mathbf{x}^{\gamma}(t)}}{dt}\Delta\mathbf{x}(t) = -\sum_{i=1}^{n}\left[Z^i(\mathbf{x}^{\gamma}(t))H_{i,\mathbf{x}^{\gamma}(t)}\Delta\mathbf{x}(t)\right]$$
$$- DF^T(\mathbf{x}^{\gamma}(t))H_{\theta,\mathbf{x}^{\gamma}(t)}\Delta\mathbf{x}(t) - H_{\theta,\mathbf{x}^{\gamma}(t)}DF(\mathbf{x}^{\gamma}(t))\Delta\mathbf{x}(t). \tag{26}$$

By noticing that

$$\frac{d}{dt}\left(H_{\theta,\mathbf{x}^{\gamma}(t)}\Delta\mathbf{x}(t)\right) = \frac{d}{dt}\left(H_{\theta,\mathbf{x}^{\gamma}(t)}\right)\Delta\mathbf{x}(t) + H_{\theta,\mathbf{x}^{\gamma}(t)}\frac{d}{dt}\left(\Delta\mathbf{x}(t)\right),$$
$$= \frac{d}{dt}\left(H_{\theta,\mathbf{x}^{\gamma}(t)}\right)\Delta\mathbf{x}(t) + H_{\theta,\mathbf{x}^{\gamma}(t)}DF(\mathbf{x}^{\gamma}(t))\Delta\mathbf{x}(t) + \mathcal{O}(|\Delta\mathbf{x}|^2), \tag{27}$$

One can rewrite Eq. (26) as

$$\frac{d}{dt}\left(H_{\theta,\mathbf{x}^{\gamma}(t)}\Delta\mathbf{x}(t)\right) = -\sum_{i=1}^{n}\left[Z^i(\mathbf{x}^{\gamma}(t))H_{i,\mathbf{x}^{\gamma}(t)}\Delta\mathbf{x}(t)\right] - DF^T(\mathbf{x}^{\gamma}(t))H_{\theta,\mathbf{x}^{\gamma}(t)}\Delta\mathbf{x}(t). \tag{28}$$

Equation (28) is valid for any perturbation $\Delta\mathbf{x}(t)$ to the limit cycle and can be used to determine $\mathbf{B}^k(\theta)$. To do so, consider the solution $\Delta\mathbf{x}(t) = \epsilon\exp(\kappa_k t)\mathbf{p}_k(\theta(t))$ taken from the structure in Eq. (12) where ϵ is small. Substituting this specific solution into (28) and recalling the relationship from Eq. (15) one can write

$$\frac{d}{dt}\left(\mathbf{B}^k(\theta(t))\epsilon\exp(\kappa_k t)\right) = -\sum_{i=1}^{n}\left[Z^i(\mathbf{x}^{\gamma}(t))H_{i,\mathbf{x}^{\gamma}(t)}\mathbf{p}_k(\theta(t))\epsilon\exp(\kappa_k t)\right] - DF^T(\mathbf{x}^{\gamma}(t))\mathbf{B}^k(\theta(t))\epsilon\exp(\kappa_k t)$$
$$\tag{29}$$

which can be manipulated to yield

$$\frac{d}{dt}\left(\mathbf{B}^k(\theta(t))\right) = -\sum_{i=1}^{n}\left[Z^i(\mathbf{x}^{\gamma}(t))H_{i,\mathbf{x}^{\gamma}(t)}\mathbf{p}_k(\theta(t))\right] - \left(DF^T(\mathbf{x}^{\gamma}(t)) + \kappa_k I\right)\mathbf{B}^k(\theta(t)). \tag{30}$$

Therefore, the function $\mathbf{B}^k(\theta(t))$ is the periodic solution to Eq. (30) subject to the normalizing condition

$$-\mathbf{Z}(\theta(t))^T DF(\mathbf{x}^{\gamma}(t))\mathbf{p}_k(\theta(t)) = \mathbf{F}(\mathbf{x}^{\gamma}(t))^T\mathbf{B}^k(\theta(t)). \tag{31}$$

Equation (31) can be derived starting with the transpose of Eq. (21) and multiplying both sides by $\mathbf{p}_k(\theta(t))$.

Following an analogous argument, starting with Eq. (20) one can derive the relation

$$\frac{d}{dt}\left(H_{\psi_j,\mathbf{x}^{\gamma}(t)}\Delta\mathbf{x}\right) = \kappa_j H_{\psi_j,\mathbf{x}^{\gamma}(t)}\Delta\mathbf{x}(t) - \sum_{i=1}^{n}\left[I_j^i(\mathbf{x}^{\gamma}(t))H_{i,\mathbf{x}^{\gamma}(t)}\Delta\mathbf{x}(t)\right] - DF^T(\mathbf{x}^{\gamma}(t))H_{\psi_j,\mathbf{x}^{\gamma}(t)}\Delta\mathbf{x}(t). \tag{32}$$

Again, choosing $\Delta\mathbf{x}(t) = \epsilon\exp(\kappa_k t)\mathbf{p}_k(\theta(t))$, and manipulating Eq. (32) one finds

$$\frac{d}{dt}\left(\mathbf{C}_j^k(\theta(t))\right) = -\sum_{i=1}^{n}\left[I_j^i(\mathbf{x}^\gamma(t))H_{i,\mathbf{x}^\gamma(t)}\mathbf{p}_k(\theta(t))\right] - \left(DF^T(\mathbf{x}^\gamma(t)) + (\kappa_k - \kappa_j)I\right)\mathbf{C}_j^k(\theta(t)). \qquad (33)$$

Therefore, the function $\mathbf{C}_j^k(\theta(t))$ is the periodic solution to Eq. (33) subject to the normalizing condition

$$\mathbf{I}_j(\theta(t))^T(\kappa_j I - DF(\mathbf{x}^\gamma(t)))\mathbf{p}_k(\theta(t)) = \mathbf{F}(\mathbf{x}^\gamma(t))^T\mathbf{C}_j^k(\theta(t)). \qquad (34)$$

Equation (34) can be derived starting with the transpose of Eq. (22) and multiplying by $\mathbf{p}_k(\theta(t))$.

Equations (30) and (33) provide a convenient strategy to solve for the necessary terms of the second order reduction from Eqs. (5) without requiring computation of the full Hessians $H_{\psi_j,\mathbf{x}^\gamma(t)}$ or $H_{\theta,\mathbf{x}^\gamma(t)}$. Furthermore, the solutions obtained from these equations do not depend on the specific choice of ϵ like for the strategy suggested by Eq. (23). The relationships from Eqs. (30) and (33) will be used as a starting point to develop strategies for the computation of phase-amplitude reduced equations in the sections to follow.

III.   ISOSTABLE REDUCTION IN NONSMOOTH DYNAMICAL SYSTEMS

The theoretical derivations presented above implicitly assume that the dynamical system from Eq. (1) is smooth, i.e., with a Jacobian $DF(\mathbf{x}^\gamma(t))$ and Hessian functions $H_{1,\mathbf{x}^\gamma(t)}, \ldots, H_{n,\mathbf{x}^\gamma(t)}$ that are defined everywhere on the limit cycle. It is not valid when the dynamics are not smooth. Such situations arise, for instance, in the modeling of cardiomyocytes where nonsmooth transitions between dynamics during systole and diastole allow for the reproduction of both cellular and tissue level characteristics of cardiac function using a small number of dynamical variables [26], [27]. Mechanical models subject to sudden impacts and dry friction are also modeled as nonsmooth systems [31]. Additionally, entrained oscillators such those that describe circadian rhythms often assume the exogenous forcing is nonsmooth [28], [29].

In cases where the dynamical system is nonsmooth, additional consideration is required in the computation of the reduced equations from Eqs. (5). The authors of [34] consider the computation of PRCs in such situations by defining jump conditions for which the PRC changes at discontinuities. As will be show here, these jump conditions along with an additional set of jump conditions for the second order terms of Eqs. (5) are required when considering nonsmooth systems.

A.   Jump Conditions for the First and Second Derivatives of the Phase Coordinate

Following the derivation for the jump conditions in the PRC presented in [34], consider an $n-1$ dimensional surface Π transverse to $\mathbf{x}^\gamma(t)$ denoting a sudden change in the dynamics of Eq. (1). On either side of Π, let the unperturbed dynamics evolve according to the smooth functions $\mathbf{F}_1(\mathbf{x})$ and $\mathbf{F}_2(\mathbf{x})$. Additionally, under the unperturbed flow of Eq. (1), assume that $\mathbf{x}^\gamma(\theta)$ crosses Π at $\theta = \theta_c$ with dynamics that transition from $\mathbf{F}_1(\mathbf{x})$ to $\mathbf{F}_2(\mathbf{x})$. In general, both $\mathbf{Z}(\theta)$ and each $\mathbf{B}^k(\theta)$ will not be continuous after this transition, and let

$$\mathbf{Z}^\alpha(\theta_*) = \lim_{\theta \to \theta_*^-}\mathbf{Z}(\theta), \qquad \mathbf{B}^{k,\alpha}(\theta) = \lim_{\theta \to \theta_*^-}\mathbf{B}^k(\theta),$$
$$\mathbf{Z}^\beta(\theta_*) = \lim_{\theta \to \theta_*^+}\mathbf{Z}(\theta), \qquad \mathbf{B}^{k,\beta}(\theta_*) = \lim_{\theta \to \theta_*^+}\mathbf{B}^k(\theta). \qquad (35)$$

Also, let $\mathbf{x}^\gamma(\theta_c)$ be the intersection of the $\mathbf{x}^\gamma(t)$ periodic orbit and the surface Π. Similar to [34] the following additional assumptions will be made: 1) θ and ψ_k for all k are continuous in an open neighborhood of $\mathbf{x}^\gamma(t)$. 2) θ and ψ_k for all k are at least twice differentiable on the interior of the two regions separated by Π. 3) Π is a hyperplane spanned by an orthonormal set of $n - 1$ vectors $\mathbf{w}_i$ for $i = 1, \ldots, n - 1$. 4) Directional derivatives of θ and ψ_k for all k exist on Π in all tangential directions.

To derive the first and second order jump conditions for $\mathbf{Z}(\theta_c)$ and $\mathbf{B}^k(\theta_c)$, consider a perturbation to the periodic orbit of the form $\mathbf{x}(t) = \mathbf{x}^\gamma(\theta(t)) + \psi_k\mathbf{p}_k(\theta(t))$, i.e., with $\psi_k = \mathcal{O}(\epsilon)$ and $\psi_j = 0$ for all $k \neq j$. Such a perturbation is represented in panel B of Figure 1. This trajectory crosses Π at a phase $\theta_c + g_k(\psi_k)$,

where $g_k(\psi_k)$ depends on the geometry of Π relative to the displacement $\mathbf{p}_k(\theta_c)$. Recalling that ψ_k and θ are assumed to be continuous, the following conditions must also be satisfied

$$[\mathbf{Z}^\alpha(\theta_c + g_k(\psi_k)) + \psi_k\mathbf{B}^{k,\alpha}(\theta_c + g_k(\psi_k))] \cdot \mathbf{w}_i =$$
$$[\mathbf{Z}^\beta(\theta + g_k(\psi_k)) + \psi_k\mathbf{B}^{k,\beta}(\theta_c + g_k(\psi_k))] \cdot \mathbf{w}_i \qquad (36)$$

for $i = 1, \ldots, n-1$. In other words, for all locations on Π the local directional derivative of the phase coordinate in all directions tangent to Π must be the identical when approaching from either side, otherwise continuity would be violated. Because $g_k(0) = 0$ asymptotically expanding g_k in powers of ψ_k results in $g_k(\psi_k) = g'_k\psi_k + \mathcal{O}(\psi_k^2)$ where $\prime \equiv d/d\psi_k$ and the derivative is evaluated at $\psi_k = 0$. Assuming that ψ_k is small, Eq. (36) can be expanded in orders of ψ_k to yield

$$\left[\mathbf{Z}^\alpha(\theta_c) + \lim_{\theta_* \to \theta_c^-} \left(\left.\frac{d\mathbf{Z}}{d\theta}\right|_{\theta=\theta_*}\right) g'_k\psi_k + \psi_k\mathbf{B}^{k,\alpha}(\theta_c)\right] \cdot \mathbf{w}_i =$$
$$\left[\mathbf{Z}^\beta(\theta_c) + \lim_{\theta_* \to \theta_c^+} \left(\left.\frac{d\mathbf{Z}}{d\theta}\right|_{\theta=\theta_*}\right) g'_k\psi_k + \psi_k\mathbf{B}^{k,\beta}(\theta_c)\right] \cdot \mathbf{w}_i + \mathcal{O}(\psi_k^2) \qquad (37)$$

Setting the $\mathcal{O}(1)$ terms equal on either side of Eq. (37) yields the relation obtained in [34]

$$\mathbf{Z}^\alpha(\theta_c) \cdot \mathbf{w}_i = \mathbf{Z}^\beta(\theta_c) \cdot \mathbf{w}_i \qquad (38)$$

for $i = 1, \ldots, n-1$. Collecting the $\mathcal{O}(\epsilon)$ terms from Eq. (37) yields the following:

$$\left[\lim_{\theta_* \to \theta_c^-} \left(\left.\frac{d\mathbf{Z}}{d\theta}\right|_{\theta=\theta_*}\right) g'_k + \mathbf{B}^{k,\alpha}(\theta_c)\right] \cdot \mathbf{w}_i = \left[\lim_{\theta_* \to \theta_c^+} \left(\left.\frac{d\mathbf{Z}}{d\theta}\right|_{\theta=\theta_*}\right) g'_k + \mathbf{B}^{k,\beta}(\theta_c)\right] \cdot \mathbf{w}_i \qquad (39)$$

for $i = 1, \ldots, n-1$. By noting that along $\mathbf{x}^\gamma(\theta)$, $\frac{d\mathbf{Z}}{d\theta} = \frac{d\mathbf{Z}}{dt}\frac{dt}{d\theta}$, and additionally using the relation given by Eq. (17) from Section II to substitute for $\frac{d\mathbf{Z}}{dt}$ and the relation $\frac{dt}{d\theta} = \frac{1}{\omega}$, Eq. (39) can be manipulated to yield

$$\left[\frac{-g'_k}{\omega} \lim_{\theta_* \to \theta_c^-} DF(\mathbf{x}^\gamma(\theta_*))^T\mathbf{Z}^\alpha(\theta_c) + \mathbf{B}^{k,\alpha}(\theta_c)\right] \cdot \mathbf{w}_i = \left[\frac{-g'_k}{\omega} \lim_{\theta_* \to \theta_c^+} DF(\mathbf{x}^\gamma(\theta_*))^T\mathbf{Z}^\beta(\theta_c) + \mathbf{B}^{k,\beta}(\theta_c)\right] \cdot \mathbf{w}_i \quad (40)$$

Conditions (38) and (40) each provide $n-1$ linearly independent conditions which will ultimately be used to determine the n components of $\mathbf{Z}$ and $\mathbf{B^k}$ after traveling through Π. In order to determine the full jump conditions, one more set of conditions will need to be derived.
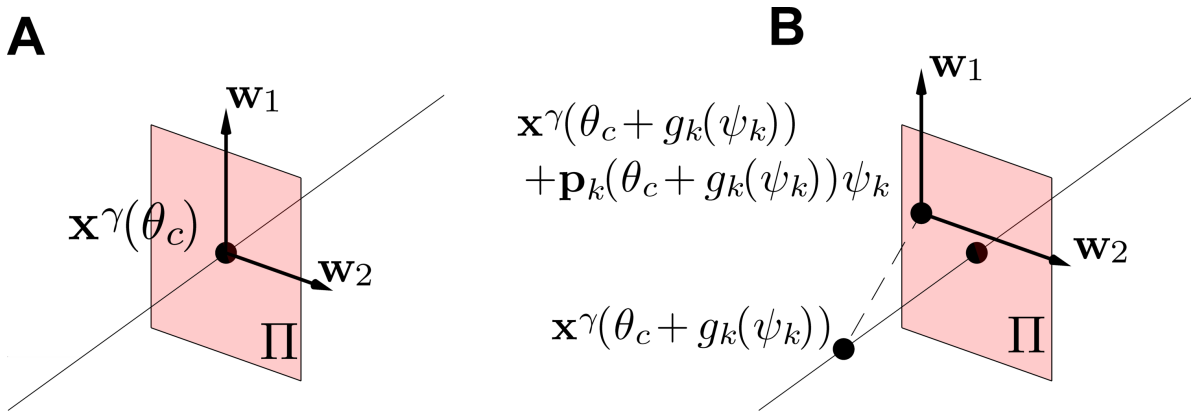

FIG. 1. In panel A, $\mathbf{x}^\gamma$ (thin line) crosses Π at a phase θ_c. In panel B, the perturbed trajectory crosses Π at $\mathbf{x}^\gamma(\theta_c + g_k(\psi_k)) + \mathbf{p}_k\psi_k$. For $\mathbf{x} \in \Pi$, local directional derivatives normal to Π approach the same value when taking the limit from either side of the surface.

One of the remaining conditions can be derived using the property of isochrons for which $\frac{\partial \theta}{\partial \mathbf{x}} \cdot \mathbf{F}(\mathbf{x}) = \omega$ for all locations in the basin of attraction of the limit cycle so that

$$\mathbf{Z}^\alpha(\theta_c) \cdot \mathbf{F}^\alpha = \omega = \mathbf{Z}^\beta(\theta_c) \cdot \mathbf{F}^\beta, \tag{41}$$

where $\mathbf{F}^\alpha \equiv \lim_{\theta \to \theta_c^-} \mathbf{F}(\mathbf{x}^\gamma(\theta))$ and $\mathbf{F}^\beta \equiv \lim_{\theta \to \theta_c^+} \mathbf{F}(\mathbf{x}^\gamma(\theta))$. For the final condition, note that the relationship from Eq. (31)

$$0 = \mathbf{Z}^T(\theta(t)) DF(\mathbf{x}^\gamma(t)) \mathbf{p}_k(\theta(t)) + \mathbf{F}^T(\mathbf{x}^\gamma(t)) \mathbf{B}^k(\theta(t)), \tag{42}$$

must hold on either side of Π. This immediately yields

$$\mathbf{Z}^\alpha(\theta_c) \cdot \lim_{\theta_* \to \theta_c^-} \left(DF(\mathbf{x}^\gamma(\theta_*)) \mathbf{p}_k(\theta_*) \right) + \mathbf{F}^\alpha \cdot \mathbf{B}^{k,\alpha}(\theta_c) = 0 =$$
$$\mathbf{Z}^\beta(\theta_c) \cdot \lim_{\theta_* \to \theta_c^+} \left(DF(\mathbf{x}^\gamma(\theta_*)) \mathbf{p}_k(\theta_*) \right) + \mathbf{F}^\beta \cdot \mathbf{B}^{k,\beta}(\theta_c). \tag{43}$$

The combination of Eqs. (38)-(41) and (43) provide the necessary constraints to determine the jump conditions on $\mathbf{Z}(\theta)$ and $\mathbf{B}^k(\theta)$ caused from the transition across Π:

$$\mathbf{Z}^\beta(\theta_c) = A_\beta^{-1} A_\alpha \mathbf{Z}^\alpha(\theta_c), \tag{44}$$
$$\mathbf{B}^{k,\beta}(\theta_c) = A_\beta^{-1} (A_\alpha \mathbf{B}^{k,\alpha}(\theta_c) + \boldsymbol{\rho}_\theta), \tag{45}$$

where

$$A_\alpha \equiv \begin{bmatrix} \mathbf{F}^\alpha & \mathbf{w}_1 & \cdots & \mathbf{w}_{n-1} \end{bmatrix}^T,$$
$$A_\beta \equiv \begin{bmatrix} \mathbf{F}^\beta & \mathbf{w}_1 & \cdots & \mathbf{w}_{n-1} \end{bmatrix}^T,$$
$$\boldsymbol{\rho}_\theta \equiv \begin{bmatrix} R_\theta^k(\theta_c) & \frac{g_k'}{\omega} \mathbf{S}_\theta(\theta_c) \cdot \mathbf{w}_1 & \cdots & \frac{g_k'}{\omega} \mathbf{S}_\theta(\theta_c) \cdot \mathbf{w}_{n-1} \end{bmatrix}^T,$$
$$R_\theta^k(\theta_c) \equiv \mathbf{Z}^\alpha(\theta_c) \cdot \lim_{\theta_* \to \theta_c^-} \left(DF(\mathbf{x}^\gamma(\theta_*)) \mathbf{p}_k(\theta_*) \right) - \mathbf{Z}^\beta(\theta_c) \cdot \lim_{\theta_* \to \theta_c^+} \left(DF(\mathbf{x}^\gamma(\theta_*)) \mathbf{p}_k(\theta_*) \right),$$
$$\mathbf{S}_\theta(\theta_c) \equiv \lim_{\theta_* \to \theta_c^+} \left(DF(\mathbf{x}^\gamma(\theta_*))^T \mathbf{Z}^\beta(\theta_c) \right) - \lim_{\theta_* \to \theta_c^-} \left(DF(\mathbf{x}^\gamma(\theta_*))^T \mathbf{Z}^\alpha(\theta_c) \right).$$

Note here that the jump condition obtained for the PRC in Eq. (44) is identical to the relation obtained in Theorem 2.2 of [34]. The authors of [34] also highlight the relationship between the jump condition described by Eq. (44) and the saltation matrix typically used as a correction for the linearized behavior of solutions resulting from a crossing of a nonsmooth boundary. For a more detailed discussion on this matter, the interested reader is referred [34].

B. Jump Conditions for the First and Second Derivatives of the Isostable Coordinate

Computing the jump conditions for $\mathbf{I}_j(\theta)$ and $\mathbf{C}_j^k(\theta)$ at $\theta = \theta_c$ is similar to the computation of the analogous functions $\mathbf{Z}(\theta)$ and $\mathbf{B}^k(\theta)$. Similar to θ, directional derivatives of ψ_k in all directions tangent to Π must be identical on either side of Π, otherwise continuity of the ψ_j coordinate would be violated. By following a similar set of steps to the previous section, by defining

$$\mathbf{I}_j^\alpha(\theta_*) = \lim_{\theta \to \theta_*^-} \mathbf{I}_j(\theta), \qquad \mathbf{C}_j^{k,\alpha}(\theta) = \lim_{\theta \to \theta_*^-} \mathbf{C}_j^k(\theta),$$
$$\mathbf{I}_j^\beta(\theta_*) = \lim_{\theta \to \theta_*^+} \mathbf{I}_j(\theta), \qquad \mathbf{C}_j^{k,\beta}(\theta_*) = \lim_{\theta \to \theta_*^+} \mathbf{C}_j^k(\theta), \tag{46}$$

In an analogous strategy to the one used in the previous section, one can use the continuity assumption on θ and ψ_j, the relation $\frac{\partial \psi_j}{\partial \mathbf{x}} \cdot \mathbf{F}(\mathbf{x}) = \kappa_j \psi_j$, and Eq. (22) to derive the jump conditions across Π:

$$\mathbf{I}_j^\beta(\theta_c) = A_\beta^{-1} A_\alpha \mathbf{I}_j^\alpha(\theta_c), \tag{47}$$
$$\mathbf{C}_j^{k,\beta}(\theta_c) = A_\beta^{-1} (A_\alpha \mathbf{C}_j^{k,\alpha}(\theta_c) + \boldsymbol{\rho}_{\psi_j}), \tag{48}$$

where

$$\boldsymbol{\rho}_{\psi_j} \equiv \left[R^k_{\psi_j}(\theta_c) \quad \frac{g'_k}{\omega} \mathbf{S}_{\psi_j}(\theta_c) \cdot \mathbf{w}_1 \quad \cdots \quad \frac{g'_k}{\omega} \mathbf{S}_{\psi_j}(\theta_c) \cdot \mathbf{w}_{n-1} \right]^T,$$

$$R^k_{\psi_j}(\theta_c) \equiv \mathbf{I}^\alpha_j(\theta_c) \cdot \lim_{\theta_* \to \theta_c^-} \left(DF(\mathbf{x}^\gamma(\theta_*)) \mathbf{p}_k(\theta_*) - \kappa_j \mathbf{p}_k(\theta_*) \right) - \mathbf{I}^\beta_j(\theta_c) \cdot \lim_{\theta_* \to \theta_c^+} \left(DF(\mathbf{x}^\gamma(\theta_*)) \mathbf{p}_k(\theta_*) - \kappa_j \mathbf{p}_k(\theta_*) \right),$$

$$\mathbf{S}_{\psi_j}(\theta_c) \equiv \lim_{\theta_* \to \theta_c^+} \left(DF(\mathbf{x}^\gamma(\theta_*))^T \mathbf{I}^\beta_j(\theta_c) - \kappa_j \mathbf{I}^\beta_j(\theta_c) \right) - \lim_{\theta_* \to \theta_c^-} \left(DF(\mathbf{x}^\gamma(\theta_*))^T \mathbf{I}^\alpha_j(\theta_c) - \kappa_j \mathbf{I}^\alpha_j(\theta_c) \right).$$

Here, A_α and A_β are defined in the previous section.

C. Application to Model of Cardiac Myocytes

For a single cardiac action potential the initial upstroke, subsequent plateau phase, and eventual repolarization is governed by a highly choreographed series of ion channel activations and deactivations. Over the past few decades, our understanding of this physiological behavior has led to the development of electrophysiological models of cardiomyocytes that incorporate upwards of 60 dynamical variables for each cell [35], [36]. While these models have become essential tools in the detailed computational study of cardiac electrophysiology they are computationally expensive to simulate and may not produce physiologically accurate results when tested with parameters outside of their intended range.

In an effort to limit the computational costs of simulating three-dimensional models with realistic geometries, minimal models for individual cardiomyocytes have been developed (e.g., [26], [27]) with parameters that can be fit to replicate tissue level characteristics of more complicated and higher dimensional models. Here the four dimensional model from [26] with external forcing will be considered so that,

$$\dot{\mathcal{U}} = -J_{fi} - J_{so} - J_{si} + u_{\text{ext}}(t),$$
$$\dot{\mathcal{V}} = (1 - H(\mathcal{U} - \theta_v))(v_\infty - \mathcal{V})/\tau_v^- - H(\mathcal{U} - \theta_v)\mathcal{V}/\tau_v^+,$$
$$\dot{\mathcal{W}} = (1 - H(\mathcal{U} - \theta_w))(w_\infty - \mathcal{W})/\tau_w^- - H(\mathcal{U} - \theta_w)\mathcal{W}/\tau_w^+,$$
$$\dot{\mathcal{S}} = ((1 + \tanh(k_s(\mathcal{U} - u_s)))/2 - \mathcal{S})/\tau_s,$$
$$\dot{t} = 1. \tag{49}$$

In the above equations, $\mathcal{U}$ is a dimensionless voltage variable which can be quantitatively related to transmembrane voltage using $V = 85.7\mathcal{U} - 84$ mV, the variables $\mathcal{U}, \mathcal{V}$, and $\mathcal{W}$ are used to determine the transmembrane currents, and $H(\cdot)$ denotes the Heaviside step function. The variable t is used to determine the external current $u_{\text{ext}}(t) = 0.3 \exp(-(\text{mod}(t, \text{BCL}) - 8)^2)$, where the basic cycle length (BCL) sets the pacing rate. Transmembrane currents, time constants, and infinity values which are functions of $\mathcal{U}$ are governed by

$$J_{fi} = -\mathcal{V}H(\mathcal{U} - \theta_v)(\mathcal{U} - \theta_v)(u_u - \mathcal{U})/\tau_{fi},$$
$$J_{so} = (\mathcal{U} - u_o)(1 - H(\mathcal{U} - \theta_w))/\tau_o + H(\mathcal{U} - \theta_w)/\tau_{so},$$
$$J_{si} = -H(\mathcal{U} - \theta_w)\mathcal{W}\mathcal{S}/\tau_{si},$$
$$\tau_v^- = (1 - H(\mathcal{U} - \theta_v^-))\tau_{v1}^- + H(\mathcal{U} - \theta_v^-)\tau_{v2}^-,$$
$$\tau_w^- = \tau_{w1}^- + (\tau_{w2}^- - \tau_{w1}^-)(1 + \tanh(k_w^-(\mathcal{U} - u_w^-)))/2,$$
$$\tau_{so} = \tau_{so1} + (\tau_{so2} - \tau_{so1})(1 + \tanh(k_{so}(\mathcal{U} - u_{so})))/2,$$
$$\tau_s = (1 - H(\mathcal{U} - \theta_w))\tau_{s1} + H(\mathcal{U} - \theta_w)\tau_{s2},$$
$$\tau_o = (1 - H(\mathcal{U} - \theta_o))\tau_{o1} + H(\mathcal{U} - \theta_o)\tau_{o2},$$
$$v_\infty = \begin{cases} 1, & \mathcal{U} < \theta_v^-, \\ 0, & \mathcal{U} \geq \theta_v^-, \end{cases}$$
$$w_\infty = (1 - H(\mathcal{U} - \theta_o))(1 - \mathcal{U}/\tau_{w\infty}) + H(\mathcal{U} - \theta_o)w_\infty^*. \tag{50}$$

In this work, the TNNP parameter set given in Table 1 of [26] will be used which replicates the behavior of the Ten Tusscher-Noble-Noble-Panfilov model [37]. Compared to more physiologically realistic models, the myocytes described by Eqs. (49) require few state variables. However, the dynamical equations use multiple

Heaviside step functions resulting in nonsmooth dynamics, making methods described in [33], [19], and [17] unusable for calculating phase and isostable response curves. The model from Eqs. (49) is piecewise smooth with transitions that occur when the variable $\mathcal{U}$ crosses the thresholds $\theta_v = 0.3$, $\theta_w = 0.015$, $\theta_v^- = 0.015$ and $\theta_o = 0.006$.

To proceed, because the pacing is periodic, t will be treated as a variable in $\mathbb{S}^1$ which takes values in the range of $[0, \text{BCL})$. Viewing from this perspective, and integrating Eqs. (49) forward in time, the dynamics settle to a stable limit cycle. If the period of oscillation is taken to be equal to BCL, three of the four non-unity Floquet multipliers are nearly zero, and the fourth is negative. In order to implement the reduction strategies described in the previous section, let $T = 2\text{BCL}$ so that all Floquet multipliers are strictly positive. Panel A of Figure 2 shows the transmembrane voltage as a function of θ along the stable limit cycle for various values of BCL. Note that even though the action potentials for larger values of BCL do indeed last longer, when plotted as a function of phase they appear shorter. Panel B shows the square root of the principle Floquet multiplier λ_1 as a function of BCL. Floquet multipliers are taken to be the eigenvalues of the fundamental matrix of the dynamical system linearized with respect to the periodic orbit (i.e., $\Delta\dot{\mathbf{x}} = DF(\mathbf{x}^\gamma(t))\Delta\mathbf{x}$). Note that as part of the computation of the fundamental matrix, saltation matrices must be used to account for the dynamical behavior induced by each nonsmooth boundary crossing [31]. As the BCL decreases, λ_1 increases towards 1; for smaller values than those shown here, alternans emerges as the result of a period doubling bifurcation [38]. The functions $\mathbf{I}_1(\theta)$ and $\mathbf{C}_1^1(\theta)$ are determined using Eqs. (18) and (32) from Section II along the with jump conditions from Eqs. (47) and (48) applied at the nonsmooth transition points. The components associated with perturbations in voltage are shown in panels C-F where $I^V(\theta) \equiv \partial\psi_i/\partial V$ and $C^V(\theta) \equiv \frac{\partial}{\partial\psi_1}\left(\frac{\partial\psi_1}{\partial V}\right)$ for different locations on the periodic orbit. Despite using different BCL values, the associated curves are relatively consistent with I^V having the largest magnitude immediately before the next action potential occurs and with C^V being largest in magnitude close to the time of repolarization, i.e., when the voltage returns to its resting value. In panels G and H, the solid lines are the same as those using BCL=340 ms from panels C and E, respectively. Dots are obtained through direct numerical simulation of Eqs. (49) using the approximations $I^V(\theta) \approx \Delta\psi_1/\Delta V$ for perturbations to initial conditions associated with the phase θ on the limit cycle and $C^V(\theta) \approx \left(\left.\frac{\Delta\psi_1}{\Delta V}\right|_{\mathbf{x}^\gamma(\theta)+\Delta\mathbf{x}} - \left.\frac{\Delta\psi_1}{\Delta V}\right|_{\mathbf{x}^\gamma(\theta)}\right)/\Delta\psi_1$ where $\Delta\mathbf{x} = \Delta\psi_1\mathbf{p}_1(\theta)$.

Finally, the effect of shifting the timing of the action potentials on the resulting transient behavior and action potential duration is investigated. Such information has been of interest for developing control strategies for eliminating cardiac alternans, a beat-to-beat alternation in the electrochemical dynamics at a cellular level [39], [40] which has been associated with the emergence of deadly arrhythmias such as cardiac arrest [41], [42]. Previous studies have shown that alternans can be suppressed by making small modifications to the timing of action potentials [43], [44], or by applying small perturbations, for instance, to the transmembrane voltage [45], [46], [47]. Conversely, alternans can be induced with variable pacing rates when the period-1 behavior is otherwise stable, for instance, with stochastic pacing [48].

For the model given by Eqs. (49), the principle isostable coordinate ψ_1 determines the length of the next action potential. For instance, if the phase starts at $\theta = 0$, a state corresponding to a positive (resp., negative) value of ψ_1 will produce a short-long-short (resp., long-short-long) pattern of action potentials. Panel A of Figure 3 shows two different trajectories where time is shifted forward (blue curve) and backwards (red curve) from an initial condition starting on the periodic orbit. Here, let Δt denote the time shift, with negative (resp., positive) values corresponding to delays (resp., advances) in the timing of the next action potential. Panels B and C show subsequent action potentials after a perturbation $\Delta t = 60$ and -60 ms, respectively. Despite the magnitude being the same, the positive shift in time results in larger amplitude alternations in the action potential duration and a slower relaxation to the limit cycle.

One can understand this discrepancy by calculating the second order accurate reduced equations corresponding to time shifts using the methods described above. Here, $I^t(\theta) \equiv \partial\psi_1/\partial t$ and $C^t(\theta) \equiv \frac{\partial}{\partial\psi_1}\left(\frac{\partial\psi_1}{\partial t}\right)$, both evaluated at $\mathbf{x}^\gamma(\theta)$ so that the second order accurate correction to the isostable response curve is $I^t(\theta) + \psi_1 C^t(\theta)$. Panel D shows a plot of this function for various values of ψ_1 and θ. To interpret this function consider a time shift $\Delta t > 0$ to an initial condition starting on the limit cycle (at $\psi_1 = 0$) occurring during the action potential at around 150 ms (approx. $\theta = 1.2$). This shift will decrease the isostable coordinate initially since $I^t(\theta) < 0$. When $\psi_1 < 0$ and $\theta \approx 1.2$, $I^t(\theta) + \psi_1 C^t(\theta) < I^t(\theta)$ so that further decreases in time will have an exacerbated effect on the isostable coordinate, working to further decrease ψ_1. Conversely, a time shift $\Delta t < 0$ will increase the isostable coordinate pushing $I^t(\theta) + \psi_1 C^t(\theta)$ closer to zero until subsequent perturbations have little effect on the isostable coordinate. Panel E shows a plot of
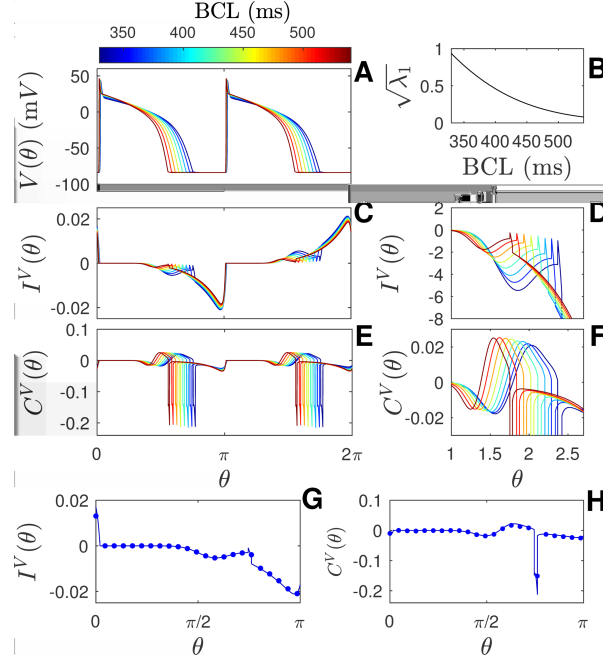
FIG. 2. Panel A shows the transmembrane voltage as a function of the phase for various values of BCL. The color of the traces corresponds to the BCL as indicated by the colorbar. In panel B, the square root of the principle Floquet multiplier, λ_1, is shown as a function of the BCL. Panel C shows $I^V(\theta)$ (the isostable response curve for voltage perturbations) and panel E shows $C^V(\theta)$ (the correction to I^V as ψ_1 changes). Panels D and F show close-ups of the curves from panels C and E, respectively, highlighting the sudden jumps across regions which are not smooth. In panels G and H the solid lines are obtained by finding the solutions to Eqs. (18) and (32) with appropriate jump conditions derived in Section III. Dots are determined by direct numerical simulation of Eqs. (49) as described in the text indicating that the numerical strategy described in Section III is accurate.

the measured (black) and expected (red) values of $\Delta\psi_1$ versus Δt, calculated from the full model equations and the second-order accurate reduced equations, respectively. A first order approximation is also shown as a dashed line. There is good agreement between the red and black curves, particularly for negative values of Δt. Neglected higher order terms begin to dominate for Δt greater than approximately 25 ms and the red and black curves begin to diverge substantially.

As a final note, an analysis of the effect on shifts in time on the action potential duration could also have been accomplished by measuring the action potential duration restitution curve [49] for this model, which gives the action potential duration as a function of the previous diastolic interval. One advantage of this method employed here, however, is that perturbations to other variables (e.g., transmembrane voltage) could also be incorporated seamlessly into the reduced model if desired. Such information could be incorporated into alternans control strategies that not only modify the timing of action potentials but also perturb the state variables themselves. Additionally, this reduction strategy could be used to characterize the influence of the pacing history on the action potential duration restitution curve, the emergence of cardiac alternans, and the breakup of spiral waves [50], [49]. The relationship between these properties of cardiac action potentials and the pacing history is referred to as memory and will be the subject of future investigation.
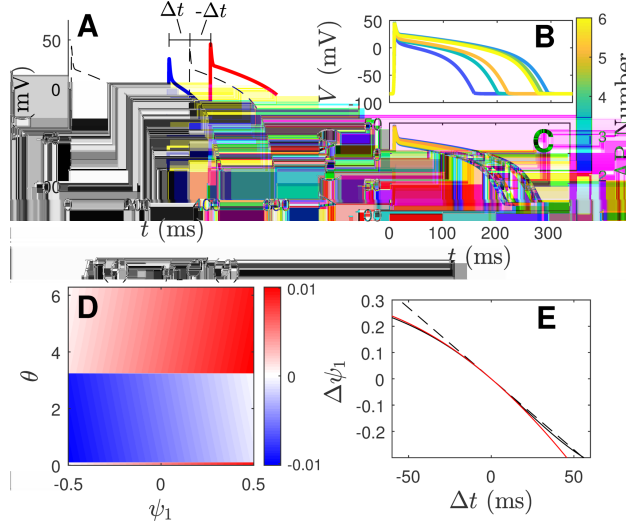
FIG. 3. In panel A, initial conditions starting on the limit cycle (black line) are perturbed by shifting time forward by 60 ms (blue line) or backward by 60 ms (red line). Panels B and C show subsequent action potentials for the forward and backward shifts in time, respectively. Despite the magnitude of each shift being identical, the perturbation caused by the forward shift takes longer to decay to the limit cycle. As described in the text, this discrepancy can be understood from the second order reduction, with $I^t(\theta) + \psi_1 C^t(\theta)$ plotted in panel D. Panel E compares the shift in ψ_1 to the time shift Δt measured from the full model given in Eqs. (49) and the reduced dynamics predicted by $I^t(\theta)$ and $C^t(\theta)$ using black and red curves respectively. The dashed line shows a first order accurate approximation for comparison (i.e., obtained taking $C^t(\theta) = 0$).

IV. ISOSTABLE COORDINATES AND REDUCTIONS FOR COMPLEX FLOQUET MULTIPLIERS

In previous sections, for the periodic solutions of the models considered Floquet multipliers were real and positive. When Floquet multipliers are complex the isostable coordinates that result from the definition in Eq. (8) are also complex and do not provide much intuition about the associated system behavior. An alternative definition for isostable coordinates when Floquet multipliers are complex is provided here which results in a real-valued coordinate system. To begin, suppose that the Floquet multipliers $\lambda_k = \sigma_k + \varphi_k i$ and $\lambda_{k+1} = \sigma_k - \varphi_k i = \lambda_k^*$ are a complex conjugate pair with corresponding eigenvectors $\mathbf{v}_k$ and $\mathbf{v}_{k+1} = \mathbf{v}_k^*$ (here * denotes the complex conjugate).

Consider the general solution of a perturbation to the periodic orbit $\mathbf{x}^\gamma(t)$ given in Eq. (12). Because λ_k is complex, the associated Floquet exponent κ_k and constant c_k will also be complex. Recall that the Floquet exponents are related to the Floquet multipliers from by $\lambda_k = \exp(\kappa_k T)$. Towards the definition of isostable coordinates for complex eigenvalues, we focus on the contributions from Eq. (12) associated with the complex Floquet multipliers λ_k and λ_k^*. When considering only these contributions, Eq. (12) becomes

$$\Delta \mathbf{x}_k(t) = \begin{bmatrix} \mathbf{p}_k(\theta(t)) & \mathbf{p}_k^*(\theta(t)) \end{bmatrix} \begin{bmatrix} y_1(t) \\ y_2(t) \end{bmatrix},$$

$$\frac{d}{dt} \begin{bmatrix} y_1 \\ y_2 \end{bmatrix} = \begin{bmatrix} \kappa_k & 0 \\ 0 & \kappa_k^* \end{bmatrix} \begin{bmatrix} y_1 \\ y_2 \end{bmatrix}, \tag{51}$$

where $y_1(0) = c_k$ and $y_2(0) = c_k^*$. By using the coordinate transformation

$$\begin{bmatrix} z_1 \\ z_2 \end{bmatrix} = \begin{bmatrix} 1 & 1 \\ -i & i \end{bmatrix} \begin{bmatrix} y_1 \\ y_2 \end{bmatrix}, \tag{52}$$

one finds

$$\frac{d}{dt} \begin{bmatrix} z_1 \\ z_2 \end{bmatrix} = \begin{bmatrix} \zeta_k & -\Omega_k \\ \Omega_k & \zeta_k \end{bmatrix} \begin{bmatrix} z_1 \\ z_2 \end{bmatrix}, \tag{53}$$

where $\zeta_k = \text{Re}(\kappa_k)$ and $\Omega_k = \text{Im}(\kappa_k)$ with initial conditions $z_1(0) = 2\text{Re}(c_k)$ and $z_2(0) = 2\text{Im}(c_k)$. Changing to polar coordinates $r = (z_1^2 + z_2^2)^{1/2}$ and $\Theta = \text{atan2}(z_2, z_1)$ where atan2 is the signed arctangent function, the dynamics become

$$\dot{r} = \zeta_k r$$
$$\dot{\Theta} = \Omega_k \tag{54}$$

with $r(0) = 2|c_k|$ and $\Theta(0) = \arg(c_k)$. The solution to Eq. (54) is simply $r(t) = r(0)\exp(\zeta_k t)$ and $\Theta(t) = \Theta(0) + \Omega_k t$. Noting that in this coordinate system, $z_1 = r\cos(\Theta)$ and that $z_2 = r\sin(\Theta)$, this implies that $z_1(t) = 2|c_k|\exp(\zeta_k t)\cos(\arg(c_k) + \Omega_k t)$ and $z_2(t) = 2|c_k|\exp(\zeta_k t)\sin(\arg(c_k) + \Omega_k t)$, and finally,

$$\Delta\mathbf{x}(t) = \begin{bmatrix} \mathbf{p}_k(\theta(t)) & \mathbf{p}_k^*(\theta(t)) \end{bmatrix} \begin{bmatrix} 1/2 & i/2 \\ 1/2 & -i/2 \end{bmatrix} \begin{bmatrix} z_1(t) \\ z_2(t) \end{bmatrix}$$
$$= 2|c_k|\exp(\zeta_k t)\left[\text{Re}(\mathbf{p}_k(\theta(t)))\cos(\Omega_k t + \arg(c_k)) - \text{Im}(\mathbf{p}_k(\theta(t)))\sin(\Omega_k t + \arg(c_k))\right]. \tag{55}$$

As an illustration of the dynamics characterized by Eq. (55), the general behavior of a three-dimensional limit cycle oscillator for which Floquet multipliers λ_1 and λ_2 are complex is shown in Figure 4. Here, the black line in panel A represents the periodic orbit, and blue ellipses represent level sets of r on the $\theta = 0$ isochron. Panel B shows 10 crossings of the $\theta = 0$ level set, which spiral in to the limit cycle.
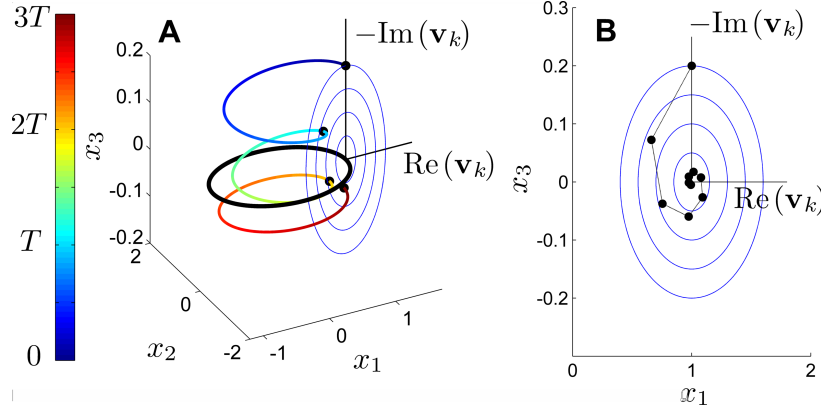

FIG. 4. General behavior of a three-dimensional limit cycle oscillator with a complex Floquet multiplier. The colored line represents three revolutions of a trajectory which starts on the $\theta = 0$ isochron that has been perturbed from the limit cycle. The black line represents the limit cycle, and black dots highlight crossings of the $\theta = 0$ level set. Blue ellipses give level sets of the variable ψ_1^M. Panel B shows the first 10 crossings of the $\theta = 0$ level set in the $x_1 x_3$-plane which spiral towards the limit cycle with subsequent crossings connected by a thin black line. In general, the value of θ_1 determines the rate of approach towards the limit cycle and larger values of φ_1 correspond to tighter spirals.

While Eq. (55) is only valid for $\mathcal{O}(\epsilon)$ perturbations from the limit cycle, this behavior allows for the definition of isostable coordinates within the entire basin of attraction. For the complex pair of Floquet multipliers $\lambda_k = \sigma_k + \varphi_k i$ and $\lambda_{k+1} = \sigma_k - \varphi_k i$, one can define two associated isostable coordinates

$$\psi_k^M = \lim_{j\to\infty}\left[\left((\chi_k^j)^2 + (\chi_{k+1}^j)^2\right)^{1/2}\exp(-\zeta_k t_\Gamma^j)\right], \tag{56}$$

$$\psi_k^P = \begin{cases} \lim_{j\to\infty}\left[\text{atan2}(\chi_{k+1}^j, \chi_k^j) - \Omega_k t_\Gamma^j\right], & \mathbf{x} \notin \mathbf{x}^\gamma, \\ 0, & \mathbf{x} \in \mathbf{x}^\gamma, \end{cases} \tag{57}$$

$$\chi_k^j = (\mathbf{w}_k^T + \mathbf{w}_{k+1}^T)(\phi(t_\Gamma^j, \mathbf{x}) - \mathbf{x}_0),$$
$$\chi_{k+1}^j = (-i\mathbf{w}_k^T + i\mathbf{w}_{k+1}^T)(\phi(t_\Gamma^j, \mathbf{x}) - \mathbf{x}_0),$$

where $\psi_k^M \in \mathbb{R}^+$ and $\psi_k^P \in [0, 2\pi)$ are the isostable magnitude and phase, respectively. Recalling that $\mathbf{w}_k^T$ and $\mathbf{w}_{k+1}^T$ are left eigenvectors corresponding to $\mathbf{v}_k$ and $\mathbf{v}_{k+1}$, and that $\mathbf{p}_k(0) = \mathbf{v}_k$, this implies that χ_k^j and

χ_{k+1}^{j} give the location in the basis $\text{Re}(\mathbf{v}_k)$ and $-\text{Im}(\mathbf{v}_k)$, respectively, at the jth return time to Γ_0 under the flow. All other functions are defined identically to those in Eq. (8). Compared to the definition from Eq. (8) which is designed for isostable coordinates associated with real Floquet multipliers, a complex Floquet multiplier requires two different coordinates. Here, ψ_k^M represents the distance from the periodic orbit along a given isochron and ψ_k^P is a phase-like coordinate. Much like the definition in Eq. (8), the amplitude-like coordinate ψ_k^M and the phase-like coordinate ψ_k^M are defined in the entire basin of attraction of the limit cycle. However, ψ_k^P is not continuously differentiable as it is discontinuous at the periodic orbit. In the analysis to follow culminating in Eq. (63) it will be shown that the coordinates obtained from Eqs. (56) and (57) are related to the coordinates obtained from the definition from Eq. (8) by the relationships $\psi_k^M = 2|\psi_k|$ and $\psi_k^P = \arg(\psi_k)$.

Direct differentiation of Eq. (56) when $\mathbf{u}(t) = 0$ yields $d\psi_k^M/dt = \zeta_k\psi_k^M$. Additionally, by direct differentiation of Eq. (57), one finds that $d\psi_k^P/dt = \Omega_k$ when $\mathbf{x} \notin \mathbf{x}^\gamma$ and behaves similarly to the asymptotic phase θ. The dynamical behavior of small perturbations from the limit cycle can also be written in terms of the phase and isostable coordinates. To do so, consider an initial condition $\mathbf{x}(0) - \mathbf{x}^\gamma(t) = \mathcal{O}(\epsilon)$ so that $\Delta\mathbf{x}(t)$ is given by Eq. (55). Substituting this directly into the equation for χ_k^j yields to leading order

$$\chi_k^j(\mathbf{x}(0)) = 2|c_k|\exp(\zeta_k t_\Gamma^j)(\mathbf{w}_k^T + \mathbf{w}_{k+1})\Big[\text{Re}(\mathbf{p}_k(\theta(t_\Gamma^j)))\cos(\Omega_k t_\Gamma^j + \arg(c_k))$$

$$- \text{Im}(\mathbf{p}_k(\theta(t_\Gamma^j)))\sin(\Omega_k t_\Gamma^j + \arg(c_k)) + \mathcal{O}(|\Delta\mathbf{x}|^2)\Big]$$

$$= 2|c_k|\exp(\zeta_k t_\Gamma^j)\cos(\Omega_k t_\Gamma^j + \arg(c_k)) + \mathcal{O}(|\Delta\mathbf{x}|^2). \tag{58}$$

Here, the second line is found using the relations $\mathbf{p}_k(\theta(t_\Gamma^j)) = \mathbf{p}_k(0) = \mathbf{v}_k$, $(\mathbf{w}_k^T + \mathbf{w}_{k+1})\text{Im}(\mathbf{v}_k) = 1$ and $(\mathbf{w}_k^T + \mathbf{w}_{k+1})\text{Re}(\mathbf{v}_k) = 0$. Similarly, one can show

$$\chi_{k+1}^j(\mathbf{x}(0)) = 2|c_k|\exp(\zeta_k t_\Gamma^j)\sin(\Omega_k t_\Gamma^j + \arg(c_k)) + \mathcal{O}(|\Delta\mathbf{x}|^2). \tag{59}$$

Using Eqs. (58) and (59) to evaluate the terms in Eqs. (56) and (57) and simplifying yields

$$\psi_k^M(0) = 2|c_k|,$$
$$\psi_k^P(0) = \arg(c_k). \tag{60}$$

Finally, substituting Eq. (60) into Eq. (55) yields

$$\Delta\mathbf{x}(t) = \psi_k^M(0)\exp(\zeta_k t)\left[\text{Re}(\mathbf{p}_k(\theta(t)))\cos(\Omega_k t + \psi_k^P(0)) - \text{Im}(\mathbf{p}_k(\theta(t)))\sin(\Omega_k t + \psi_k^P(0))\right] + \mathcal{O}(|\Delta\mathbf{x}|^2),$$
$$= \psi_k^M(t)\left[\text{Re}(\mathbf{p}_k(\theta(t)))\cos(\psi_k^P(t)) - \text{Im}(\mathbf{p}_k(\theta(t)))\sin(\psi_k^P(t))\right] + \mathcal{O}(|\Delta\mathbf{x}|^2), \tag{61}$$

where the second line is obtained by using the relations $\psi_k^M(t) = \psi_k^M(0)\exp(\zeta_k t)$ and $\psi_k^P(t) = \psi_k^P(0) + \Omega_k t$. Equation (61) is valid for all ψ_k^M and ψ_k^P provided that the state is close enough to the limit cycle and gives a relationship between the isostable and phase coordinates when all isostable coordinates except ψ_k^M and ψ_k^P are identical to zero.

More generally, if one consider a limit cycle oscillator for which there are both real and imaginary eigenvalues of J_p, ordering eigenvalues so that λ_j are complex for $j = 1, \ldots, 2q$, real-valued for $j = 2q+1, \ldots, n-1$, and $\lambda_n = 1$ (corresponding to the periodic orbit) one can write

$$\Delta\mathbf{x} = \sum_{k=1}^{q}\psi_{2k-1}^M\left[\text{Re}(\mathbf{p}_{2k-1}(\theta))\cos(\psi_{2k-1}^P) - \text{Im}(\mathbf{p}_{2k-1}(\theta))\sin(\psi_{2k-1}^P)\right],$$

$$+ \sum_{k=2q+1}^{n-1}\psi_k\mathbf{p}_k(\theta), \tag{62}$$

where the explicit dependence on t of each of the variables has been dropped for notational convenience. In Eq. (62), ψ_k^M and ψ_k^P are defined using Eqs. (56) and (57) for $k = 1, 3, \ldots, 2q-1$ and the remainder of the isostable coordinates ψ_k are defined using Eq. (8).

A. Phase-Amplitude Reduction with Complex Floquet Multipliers

Here a phase-amplitude reduction similar to Eqs. (5) using the isostable coordinates ψ_k^M and ψ_k^P is described. For clarity in the presentation of this section, it is assumed that the limit cycle has one Floquet multiplier equal to 1, two complex conjugate Floquet multipliers λ_k and λ_k^* and that for the remaining Floquet multipliers $0 < |\lambda_k| \ll 1$, remaining Floquet multipliers that are close enough to zero so that they can be ignored in the reduction. The analysis to follow could be adapted to situations where there are multiple complex and non-complex Floquet multiplers which cannot be neglected.

For this system, the methodology from Section II can be used to compute the terms in the reduction given in Eqs. (5). However, the resulting functions $\mathbf{B}^k(\theta)$, $\mathbf{I}_j(\theta)$, $\mathbf{C}_j^k(\theta)$ and isostable coordinates themselves will be complex-valued making it difficult to develop intuition about the system dynamics. Here, Eqs. (5) will serve as a starting point for determining a reduction using the coordinates ψ_1^M and ψ_1^P as defined in the previous section.

To begin, suppose that all the functions in the reduction given by Eqs. (5) have already been calculated. As illustrated in [19], for small perturbations Δx from the limit cycle, c_1 from Eq. (12) is well approximated by ψ_1. Additionally, recall for small Δx, Eq. (60) states that $\psi_1^M(0) = 2|c_1|$ and $\psi_1^P(0) = \arg(c_1)$. This information taken together, along with the fact that isostable coordinates are determined by the infinite time approach of trajectories to the periodic orbit implies the following relations:

$$\psi_1^M = 2|\psi_1|,$$
$$\psi_1^P = \arg(\psi_1),$$
$$\mathrm{Re}(\psi_1) = \frac{1}{2}\psi_1^M \cos(\psi_1^P),$$
$$\mathrm{Im}(\psi_1) = \frac{1}{2}\psi_1^M \sin(\psi_1^P). \tag{63}$$

Recalling that $|\psi_1| \equiv \sqrt{\mathrm{Re}(\psi_1)^2 + \mathrm{Im}(\psi_1)^2}$, direct differentiation of the above relationships yields

$$\frac{\partial \psi_1^M}{\partial x} = \frac{2}{|\psi_1|}\left[\mathrm{Re}(\psi_1)\mathrm{Re}\left(\frac{\partial \psi_1}{\partial x}\right) + \mathrm{Im}(\psi_1)\mathrm{Im}\left(\frac{\partial \psi_1}{\partial x}\right)\right]$$
$$= 2\left[\cos(\psi_1^P)\mathrm{Re}\left(\frac{\partial \psi_1}{\partial x}\right) + \sin(\psi_1^P)\mathrm{Im}\left(\frac{\partial \psi_1}{\partial x}\right)\right], \tag{64}$$
$$\frac{\partial \psi_1^P}{\partial x} = \frac{1}{\mathrm{Re}(\psi_1)^2}\left[\mathrm{Re}(\psi_1)\mathrm{Im}\left(\frac{\partial \psi_1}{\partial x}\right) - \mathrm{Im}(\psi_1)\mathrm{Re}\left(\frac{\partial \psi_1}{\partial x}\right)\right],$$
$$= \frac{2}{\psi_1^M}\left[\cos(\psi_1^P)\mathrm{Im}\left(\frac{\partial \psi_1}{\partial x}\right) - \sin(\psi_1^P)\mathrm{Re}\left(\frac{\partial \psi_1}{\partial x}\right)\right], \tag{65}$$

where the second lines in the above equations are obtained by using relations from Eqs. (63). Note that Eq. (65) requires $\psi_1^M \neq 0$, otherwise $\arg(\psi_1)$ is undefined and the derivative does not exist. Continuing to expand Eq. (64) using information from the already computed reduction given by Eqs. (5),

$$\frac{\partial \psi_1}{\partial x} = \mathbf{I}_1(\theta) + \mathbf{C}_1^1(\theta)\psi_1 + \mathbf{C}_1^2(\theta)\psi_2$$
$$= \mathbf{I}_1(\theta) + \mathbf{C}_1^1(\theta)\psi_1 + \mathbf{C}_1^2(\theta)\psi_1^*$$
$$= \mathbf{I}(\theta) + i\left[\mathrm{Re}(\mathbf{C}_1^1(\theta))\mathrm{Im}(\psi_1) + \mathrm{Im}(\mathbf{C}_1^1(\theta))\mathrm{Re}(\psi_1) + \mathrm{Im}(\mathbf{C}_1^2(\theta))\mathrm{Re}(\psi_1) - \mathrm{Re}(\mathbf{C}_1^2(\theta))\mathrm{Im}(\psi_1)\right]$$
$$+ \left[\mathrm{Re}(\mathbf{C}_1^1(\theta))\mathrm{Re}(\psi_1) - \mathrm{Im}(\mathbf{C}_1^1(\theta))\mathrm{Im}(\psi_1) + \mathrm{Re}(\mathbf{C}_1^2(\theta))\mathrm{Re}(\psi_1) + \mathrm{Im}(\mathbf{C}_1^2(\theta))\mathrm{Im}(\psi_1)\right] \tag{66}$$

where the relationship $\psi_1^* = \psi_2$ used in line 2 can be verified for all real-valued initial conditions from Eq. (8) by noting that $\mathbf{w}_1^* = \mathbf{w}_2$ for complex conjugate Floquet multipliers $\lambda_1^* = \lambda_2$. Substituting Eq. (66)

into Eq. (64) and simplifying the resulting relation using Eqs. (63) yields

$$
\begin{aligned}
\frac{\partial \psi_1^M}{\partial x} &= \mathbf{I}_{1,M}(\theta, \psi_1^P) + \psi_1^M \mathbf{C}_{1,M}^1(\theta, \psi_1^M), \\
\mathbf{I}_{1,M}(\theta, \psi_1^P) &\equiv 2 \left[\cos(\psi_1^P)\mathrm{Re}(\mathbf{I}_1(\theta)) + \sin(\psi_1^P)\mathrm{Im}(\mathbf{I}_1(\theta)) \right], \\
\mathbf{C}_{1,M}^1(\theta, \psi_1^P) &\equiv \cos^2(\psi_1^P)(\mathrm{Re}(\mathbf{C}_1^1(\theta)) + \mathrm{Re}(\mathbf{C}_1^2(\theta)) + \sin^2(\psi_1^P)(\mathrm{Re}(\mathbf{C}_1^1(\theta)) - \mathrm{Re}(\mathbf{C}_1^2(\theta)) \\
&\quad + 2\sin(\psi_1^P)\cos(\psi_1^P)\mathrm{Im}(\mathbf{C}_1^2(\theta)).
\end{aligned}
\tag{67}
$$

Next, starting with Eq. (65), substituting Eq. (66), and simplifying yields,

$$
\begin{aligned}
\frac{\partial \psi_1^P}{dx} &= \frac{1}{\psi_1^M}\mathbf{I}_{1,P}(\theta, \psi_1^P) + \mathbf{C}_{1,P}^1(\theta, \psi_1^P), \\
\mathbf{I}_{1,P}(\theta, \psi_1^P) &\equiv 2 \left[\cos(\psi_1^P)\mathrm{Im}(\mathbf{I}_1(\theta)) - \sin(\psi_1^P)\mathrm{Re}(\mathbf{I}_1(\theta)) \right], \\
\mathbf{C}_{1,P}^1 &\equiv \cos^2(\psi_1^P)(\mathrm{Im}(\mathbf{C}_1^1(\theta)) + \mathrm{Im}(\mathbf{C}_1^2(\theta))) + \sin^2(\psi_1^P)(\mathrm{Im}(\mathbf{C}_1^1(\theta)) - \mathrm{Im}(\mathbf{C}_1^2(\theta))) \\
&\quad - 2\sin(\psi_1^P)\cos(\psi_1^P)\mathrm{Re}(\mathbf{C}_1^2(\theta)).
\end{aligned}
\tag{68}
$$

Finally, considering the gradient of the phase coordinate

$$
\begin{aligned}
\frac{\partial \theta}{\partial x} &= \mathbf{Z}(\theta) + \psi_1 \mathbf{B}^1(\theta) + \psi_2 \mathbf{B}^2(\theta), \\
&= \mathbf{Z}(\theta) + \psi_1 \mathbf{B}^1(\theta) + \psi_1^* (\mathbf{B}^1(\theta))^*, \\
&= \mathbf{Z}(\theta) + 2\mathrm{Re}(\psi_1 \mathbf{B}^1(\theta)), \\
&= \mathbf{Z}(\theta) + 2 \left[\mathrm{Re}(\psi_1)\mathrm{Re}(\mathbf{B}^1(\theta)) - \mathrm{Im}(\psi_1)\mathrm{Im}(\mathbf{B}^1(\theta)) \right], \\
&= \mathbf{Z}(\theta) + \psi_1^M \mathbf{B}_c^1(\theta, \psi_1^P),
\end{aligned}
\tag{69}
$$

with $\mathbf{B}_c^1(\theta, \psi_1^P) \equiv \cos(\psi_1^P)\mathrm{Re}(\mathbf{B}^1(\theta)) - \sin(\psi_1^P)\mathrm{Im}(\mathbf{B}^1(\theta))$. In the second line of the equation above, the relationship $\mathbf{B}^2(\theta) = (\mathbf{B}^1(\theta))^*$ is used; this relationship can be found by contradiction by first assuming that $\mathbf{B}^2(\theta) \neq (\mathbf{B}^1(\theta))^*$. If this were true, then a small and real perturbation Δx to the state would yield a phase coordinate with a non-zero imaginary component which results in a contradiction.

Together, Eqs. (67)-(69) can be used to determine the phase-amplitude reduced equation for a system with a complex Floquet multiplier:

$$
\begin{aligned}
\dot{\theta} &= \omega + \left[\mathbf{Z}(\theta) + \psi_1^M \mathbf{B}_c^1(\theta, \psi_1^P) \right] \cdot \mathbf{u}(t), \\
\dot{\psi}_1^M &= \zeta_1 \psi_1^M + \left[\mathbf{I}_{1,M}(\theta, \psi_1^P) + \psi_1^M \mathbf{C}_{1,M}^1(\theta, \psi_1^M) \right] \cdot \mathbf{u}(t), \\
\dot{\psi}_1^P &= \Omega_1 + \left[\frac{1}{\psi_1^M}\mathbf{I}_{1,P}(\theta, \psi_1^P) + \mathbf{C}_{1,P}^1(\theta, \psi_1^P) \right] \cdot \mathbf{u}(t),
\end{aligned}
\tag{70}
$$

where the unperturbed dynamics (i.e., when $\mathbf{u} = 0$) were derived early in Section IV. Note that the ψ_1^P dynamics require $\psi_1^M \neq 0$ as emphasized earlier. In situations where high accuracy approximations of the dynamics are not necessary, a truncated version of Eqs. (70) can be used (similar to the first order accurate isostable reduction suggested by [17] for real-valued Floquet multipliers)

$$
\begin{aligned}
\dot{\theta} &= \omega + \mathbf{Z}(\theta) \cdot \mathbf{u}(t), \\
\dot{\psi}_1^M &= \zeta_1 \psi_1^M + \mathbf{I}_{1,M}(\theta, \psi_1^P) \cdot \mathbf{u}(t), \\
\dot{\psi}_1^P &= \Omega_1 + \frac{1}{\psi_1^M}\mathbf{I}_{1,P}(\theta, \psi_1^P) \cdot \mathbf{u}(t).
\end{aligned}
\tag{71}
$$

Finally, the above phase-amplitude reduction can be adapted straightforwardly for systems with both real and imaginary Floquet multipliers by defining the isostable coordinates associated with each Floquet multiplier appropriately.

B. Example Reduction with Complex Floquet Multipliers

To illustrate the phase-amplitude reduction using isostable coordinates, the canonical nonlinear model of a pendulum [25] with external, time-dependent forcing, viscous damping, and an external torque will be considered

$$\dot{X}_1 = X_2,$$
$$\dot{X}_2 = \frac{F_{\text{ext}}(t)\cos(X_1)}{mL} - \frac{g}{L}\sin(X_1) - \frac{K}{mL^2}X_2 + \frac{u(t)}{mL^2}. \tag{72}$$

Here $X_1 \in \mathbb{S}^1$ and $X_2 \in \mathbb{R}$ correspond to the angular position and velocity of the pendulum, respectively, $m = 1$ Kg represents a point mass suspended by a massless rod of length $L = 5$ meters, $g = 9.8\text{m/s}^2$ is the acceleration due to gravity, $K = 1\frac{\text{Nm}}{(\text{rad}/s)}$ is the viscous damping coefficient, and $F_{\text{ext}}(t) = 5\sin(\frac{2\pi t}{T})$ Newtons is a periodic horizontal force with a period of $T = 3$ seconds, and $u(t)$ is a controlling torque. A schematic of Eq. (72) is shown in panel A of Figure 5.

As illustrated in [51], Eqs. (72) can be rewritten as an autonomous set of ordinary differential equations,

$$\dot{X}_1 = X_2,$$
$$\dot{X}_2 = \frac{5\sin(\frac{2\pi X_3}{T})\cos(X_1)}{mL} - \frac{g}{L}\sin(X_1) - \frac{K}{mL^2}X_2 + \frac{u(t)}{mL^2},$$
$$\dot{X}_3 = 1, \tag{73}$$

where $X_3 \in \mathbb{S}^1$ is a time-like variable which takes values in the range $[0, T)$. For the moment Eqs. (73) will be analyzed taking $u(t) = 0$. For the choice of parameters used here, Eqs. (73) admit a stable limit cycle with complex, non-unity Floquet multipliers $\lambda_1 = -0.674 + 0.658i$, $\lambda_2 = \lambda_1^*$, with corresponding right eigenvectors $v_1 = \begin{bmatrix} -0.012 + 0.626i & 0.779 & 0 \end{bmatrix}^T$, $v_2 = v_1^*$, and $\kappa_1 = -0.02 + 0.789i$ so that $\zeta_1 = -0.02$ and $\Omega_1 = 0.789$. Two sample trajectories with initial conditions $X_1(0) = -2.2$ rad, $X_2(0) = -0.2$ rad/s and $X_3(0) = 0$ s are shown in panels B and C of Figure 5. After some initial transient behavior, the state settles close to the periodic orbit, however, this happens relatively slowly since $|\lambda_1| = 0.942$. The coordinates ψ_1^M and ψ_1^P can be calculated using the definitions from Eqs. (56) and (57), respectively, and are shown for different cross sections of X_3 in panels D and E. Some initial conditions (shown in white) do not converge to the limit cycle, but rather to other attractors (c.f., [52]). In this example, because the pendulum receives an external time dependent forcing, the phase is only dependent on the variable X_3 and the relationship $\theta(t) = \frac{2\pi X_3(t)}{T}$ can be used to relate the X_3 coordinate to the isochrons. Thus, the cross sections in panes D and E represent level sets of the isochrons. For locations that are farther from the periodic orbit (for instance, $(X_1, X_2, X_3) \approx (-3, 2, 0)$ small changes in the initial conditions generally lead to large differences in the transient behavior, particularly in the time it takes the pendulum to settle to its periodic orbit giving the appearance of static in the cross sections.

The reduction strategy detailed in Section IV A is applied to the forced pendulum represented by Eqs. (73). In this example, since the original system from Eqs. (73) has only 3 state variables, using phase and isostable coordinates does not result in a reduction in dimensionality, and is perhaps more accurately described as a transformation. Nevertheless, it is still instructive to view this system from the perspective of isostable coordinates. The numerically calculated functions used in this reduction are shown in Figure 6. Panels A and B give color plots of $\mathbf{I}_{1,M}(\theta, \psi^P)$ and $\mathbf{C}_{1,M}^1(\theta, \psi^P)$ from Eqs. (70), respectively. Panels C, D, and E, show related functions evaluated along a trajectory for which $\theta(t) = \omega t$ and $\psi_1^P(t) = \Omega_1 t$. In general, unlike the isostable reduction that results from Floquet multipliers, the functions displayed in panels C, and E are quasiperiodic (unless Ω_1/ω is rational). Additionally, the magnitude of $\partial \psi_1^P/\partial X_2$ grows as the isostable coordinate continues to shrink, approaching infinity as ψ_1^M approaches 0.

To illustrate the utility of the reduced coordinate system, a relatively simple control strategy will be investigated with the goal of stabilizing the limit cycle of Eqs. (73) in the presence of noise. To incorporate noise, a Gaussian white noise process with zero-mean and variance 0.16 is added to the equation for $\dot{X}_2$. This noise process mimics the the effect of a noisy torque applied to the pendulum. Panel A of Figure 7 shows a representative simulation of Eqs. (73) with noise added. Despite the noise amplitude being relatively small, it can have a significant effect on the system because $|\lambda_1|$ is close to 1. Using an initial condition with at $\theta = 0$ on the limit cycle, the noise quickly drives the state far from the limit cycle and the pendulum makes
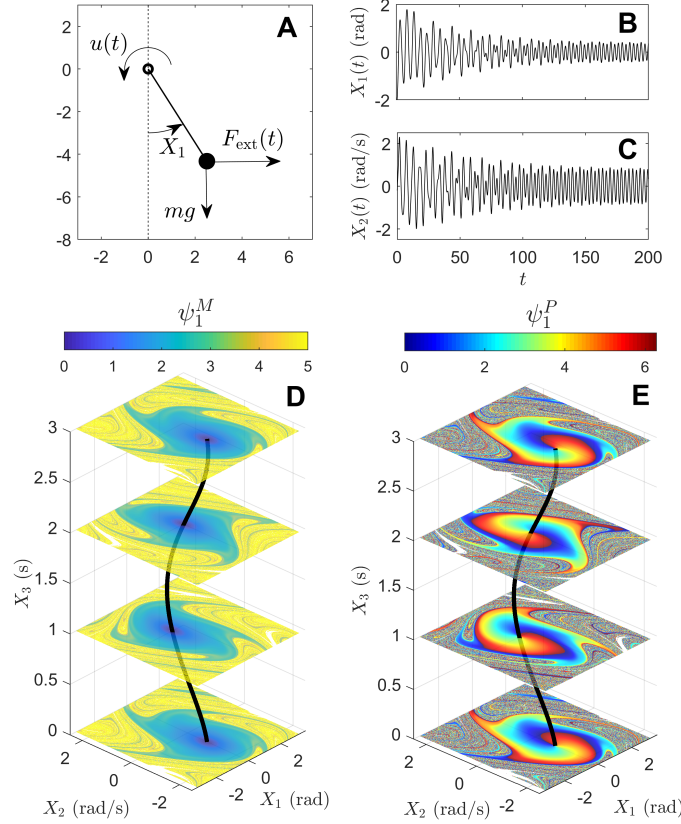
FIG. 5. Panel A shows a schematic for the forced pendulum represented by Eqs. (72) with an example trajectory shown in panels B and C. The isostable coordinates ψ_1^M and ψ_1^P are calculated for this system and shown in panels D and E, respectively, where the solid black line shows the stable limit cycle of Eqs. (73). The ψ_1^M coordinate gives a sense of how long it will take a given initial condition to approach the periodic orbit. Notice that locations where the limit cycle intersects each X_3 cross section correspond to isostable coordinates $\psi_1^M = \psi_1^P = 0$.

multiple full revolutions. In an effort to stabilize the limit cycle in the presence of noise, a controlling torque $u(t)$ will be added with a relatively simple control strategy

$$u(t) = \begin{cases} u_{\max}, & \text{if } I_{1,M}^{X_2}(\theta, \psi_1^P) < 0 \text{ and } \psi_1^M > \psi_{\text{thresh}}^M, \\ -u_{\max}, & \text{if } I_{1,M}^{X_2}(\theta, \psi_1^P) \geq 0 \text{ and } \psi_1^M > \psi_{\text{thresh}}^M, \\ 0, & \text{if } \psi_1^M \leq \psi_{\text{thresh}}^M, \end{cases} \tag{74}$$

where $u_{\max} > 0$ is the maximum magnitude of the controlling torque, and ψ_{thresh}^M is some threshold under which no control is applied, and $I_{1,M}^{X_2}(\theta, \psi_1^P)$ denotes the component of $\mathbf{I}_{1,M}(\theta, \psi_1^P)$ associated with perturbations to X_2. The control policy given in Eq. (74) results in a bang-off-bang controller [53] which seeks to maximally decrease the value of ψ_1^M when it is larger than the prescribed threshold. The switching point is chosen using Eqs. (70) to give a perturbation which will drive ψ_1^M towards more negative values as rapidly as possible.

In order to implement the control strategy from Eqs. (74) it is necessary to have an estimate of the coordinates ψ_1^M and ψ_1^P. To do so, it is assumed that the system always stays close to the limit cycle solution when the control strategy is active and allow for the direct measurement of the state every T seconds (i.e., once per period). This periodic measurement is used to approximate c_1 and c_2 from Eq. (12) which in turn are used to estimate the isostable coordinates according to Eqs. (63). At all other times the controller estimates of the phase and isostable dynamics assuming that the noise intensity is zero according
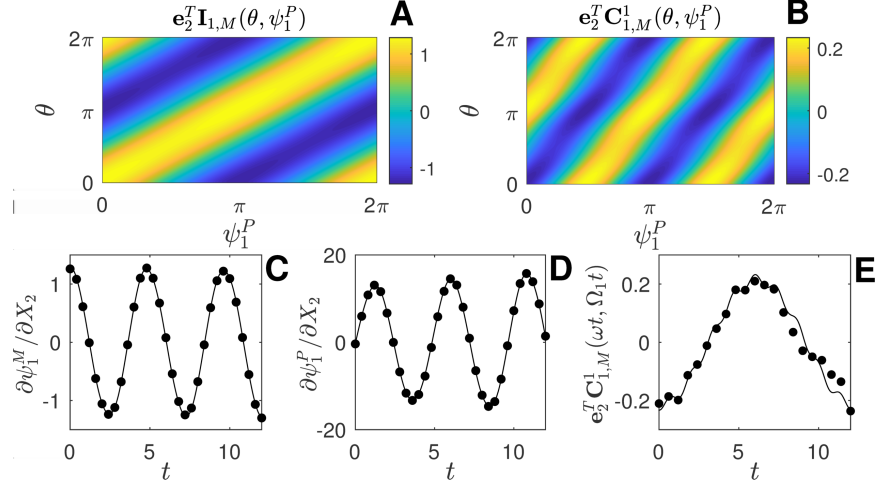
FIG. 6. As part of the terms of the phase-amplitude reduction of the forced pendulum in Eqs. (73), panels A and B show the components of $\mathbf{I}_{1,M}(\theta,\psi_1^P)$ and $\mathbf{C}_{1,M}^1(\theta,\psi_1^P)$, respectively, associated with perturbations to X_2 (here $\mathbf{e}_2^T \equiv [0\ 1\ 0]$). Panels C, D, and E show specific components of the reduced equations evaluated along an unperturbed trajectory $\mathbf{x}(t)$ with initial coordinates $[\theta,\psi_1^M,\psi_1^P] = [0,0.1,0]$. Solid lines correspond to the value obtained using the computational strategy from Section IV A; the dots are obtained directly using the approximation $\partial\psi_1^M/\partial X_2 \approx \Delta\psi_1^M/\Delta X_2$ and $\partial\psi_1^P/\partial X_2 \approx \Delta\psi_1^P/\Delta X_2$ for small perturbations ΔX_2. In panel E the dots are obtained directly with the approximation $\mathbf{e}_2^T \mathbf{C}_{1,M}^1(\omega t, \Omega_1 t) \approx \left(\left.\frac{\Delta\psi_1^M}{\Delta X_2}\right|_{\mathbf{x}_p(t)} - \left.\frac{\Delta\psi_1^M}{\Delta X_2}\right|_{\mathbf{x}(t)} \right) / (\exp(\zeta_1 t)\Delta\psi_1^M)$, where $\mathbf{x}_p(t)$ is an unperturbed trajectory with initial coordinates $[0,\psi_1^M,\psi_1^P] = [0,0.1+\Delta\psi_1^M,0]$.
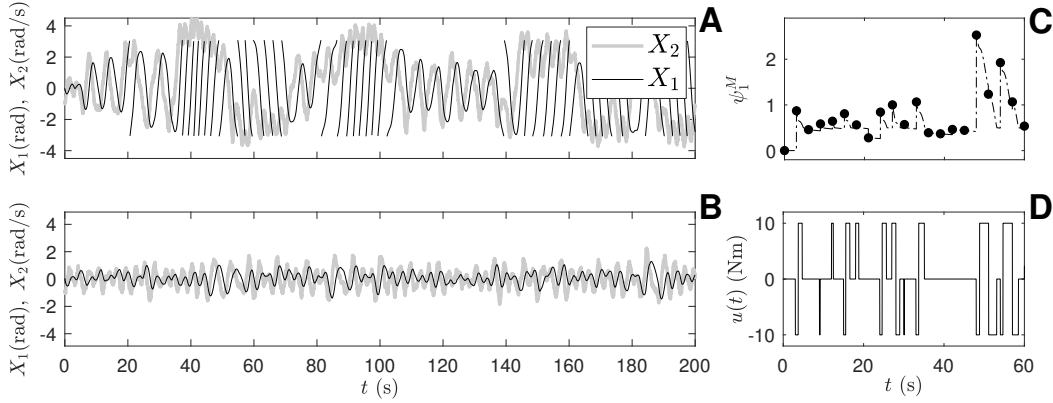

FIG. 7. Panel A shows 200 seconds of simulated data using Eqs. (73) where $u(t) = 0$ with noise added as described in the text. The noise quickly destabilizes the limit cycle allowing the pendulum to make full revolutions past $X_1 = \pi$. Panel B shows the same system with the control strategy given by Eq. (74) applied. Panels C shows the internal estimate of $\psi_1^M(t)$ as a dot-dashed line with black dots inferred from measurements of the state as described in the text. Panel D gives an example of the applied control.

to Eqs. (71). For this internal estimate, it is assumed that the noise intensity is small enough so that higher order terms from the Ito correction are negligible [54], [55]. Additionally, this estimate is updated when state measurements are taken every T seconds to account for the drift due to noise that is not considered by the controller.

Panel B of Figure 7 shows the result of applying the control strategy from Eq. (74) to the system given by Eqs. (73) (with noise added to the $\dot{X}_2$ equation as described earlier. Using $\psi_{\max}^M = 0.5$ and $u_{\max} = 10$Nm. Compared to the uncontrolled case, the motion is much more regular and the state does not deviate

substantially from the stable limit cycle. Panel C shows the internal estimate for $\psi_1^M(t)$ over the first 60 seconds of simulation. The dots indicate estimates that come from measurements of the state every T seconds, and the dashed-dotted line represents the intermediate state estimates. Panel D shows the applied control over the first 60 seconds. Because the noise that is not accounted for in the internal state estimate, the difference between the actual state and the estimate can grow substantially between direct measurements, resulting in the large jumps observed in panel C. Despite this mismatch, however, the controller still does quite well at maintaining reasonably small values of ψ_1^M in these simulations. Indeed, over the course of 3000 seconds of simulation, the mean and standard deviation of the estimated value of ψ_1^M is 0.68 and 0.41, respectively. Conversely, in the uncontrolled case over the same time frame, the mean and standard deviation is 2.87 and 1.59, respectively.

V. DISCUSSION AND CONCLUSION

For many decades, phase reduction has been an essential tool in the analysis of weakly perturbed nonlinear limit cycle oscillators, particularly when questions about timing, synchronization, and entrainment are of interest [7], [2], [3]. In situations where information about the dynamics in directions transverse to the periodic orbit are of interest, phase-amplitude reduction using the notion of isostable coordinates to augment the standard phase reduction given by Eq. (4) is also useful [17] and has allowed for the development of more accurate reduced equations [19] for use with larger perturbations. In this work, strategies are developed to apply this reduction methodology to dynamical systems that are piecewise smooth and to systems with limit cycles that have complex Floquet multipliers.

For the computation of the terms of the second order accurate reduction from Eqs. (5) for limit cycle oscillators with piecewise smooth dynamics, it is essential to characterize the discontinuities in $\mathbf{Z}(\theta)$, $\mathbf{I}_j(\theta)$, $\mathbf{B}^k(\theta)$ and $\mathbf{C}_j^k(\theta)$ associated with crossing a boundary where the vector field $\mathbf{F}(\mathbf{x})$ is discontinuous. The jump conditions associated with these boundary crossings are related to the saltation matrix and derived in [34] for the computation of PRCs in piecewise smooth dynamical systems. Using a similar approach in Section III, the jump conditions for the computation of the IRCs and each $\mathbf{B}^k(\theta)$ and $\mathbf{C}_j^k(\theta)$ are derived. Using these jump conditions, one can calculate all of the terms of the reduction from Eqs. (5). This strategy is applied to analyze the behavior of a model of human ventricular myocytes given in Eqs. (49) with a reduced framework. In the resulting reduction, the principle isostable coordinate ψ_1 is associated with the severity of alternans observed in response to perturbations from the nominal limit cycle. The reduction implemented here suggests the possibility of developing a unified framework which could be used in control strategies for the elimination of alternans incorporating both direct perturbations to the system's state (like in [45], [46], [47]) and changes in the nominal timing of the action potentials (like in [43], [44]). Additionally, similar reduction methodologies could be applied to investigate entrainment in circadian systems to a light source which is large in magnitude, but switched on and off suddenly [28], [29]. In this context, the isostable coordinates could be used to characterize the level of circadian misalignment due to shifts in time due to travel across multiple time zones; this framework could be used to study the effect subsequent perturbations on the subsequent reentrainment to the new time zone.

In previous work [19], the definition of isostable coordinates from Eq. (8) is difficult to visualize and provides little intuition about the underlying system when Floquet multipliers take complex values. In this work, a new definition for isostable coordinates associated with complex-valued Floquet multipliers is developed. Each complex conjugate pair of Floquet multipliers λ_k and λ_k^* is associated with two isostable coordinates ψ_k^M and ψ_k^P defined in Eqs. (56) and (57), respectively. Near the periodic orbit, on a given isochron, level sets of ψ_M are well approximated by ellipses, with ψ_k^M corresponding to the location on a given ellipse. The resulting reduced equations given by Eq. (70) when using ψ_k^M and ψ_k^P coordinates is different than the reduction from Eqs. (5) for Floquet multipliers that are real-valued. Additionally, the gradient of ψ_k^P approaches infinity as ψ_k^M approaches zero (i.e., as the state approaches the limit cycle) leading to difficulties when working with reduced Eqs. (70) and (71) when the state is near the periodic orbit. The transformation to isostable coordinates resulting in the reduction from Eqs. (71) is illustrated in a canonical model of a chaotic forced pendulum. For this particular system, the use of phase and isostable coordinates does not reduce the overall dimension of the dynamical system, but it does provide the necessary intuition to implement a straightforward simple control strategy to stabilize the behavior of the pendulum's behavior in the presence of noise. Additionally, this method can be straightforwardly applied to dynamical systems with higher dimension than in the applications considered here.

The reductions from Eqs. (5) and (70) provide a correction for the dynamical behavior as the state of a dynamical system becomes farther from its periodic orbit which is more accurate than the standard phase reduction given by Eq. (4) which discards all information about the dynamics transverse to the periodic orbit. However, as part of the reductions given by Eqs. (5) and (70), higher order terms of the asymptotic expansion to the gradient of the phase and isostable coordinates near the periodic orbit are still truncated. As such, the state must still remain reasonably close to the limit cycle so that Eqs. (5) and (70) remain valid. For this reason, others have investigated the possibility of calculating phase and amplitude coordinates in $\mathbb{R}^n$ [56], [57], [58], however, this is difficult to accomplish numerically for models of more than $n = 4$ dimensions and ultimately does not reduce the number of state variables which must be considered.

Limit cycle oscillators with piecewise smooth dynamics which have been used to replicate the essential features of complicated dynamical systems such as cardiomyocytes [26], [27] and neurons [30], and circadian oscillators [28], [29]. Additionally, the limit cycles often have complex-valued Floquet multipliers in applications where external forcing is applied. The methods presented here allow for the phase-amplitude reduction of these types of systems using isostable coordinates, allowing for their study in a more convenient framework.

[1] A. B. Holt and T. I. Netoff. Origins and suppression of oscillations in a computational model of Parkinsons disease. *Journal of Computational Neuroscience*, 37(3):505–521, 2014.

[2] F. C. Hoppensteadt and E. M. Izhikevich. *Weakly Connected Neural Networks*. Springer, New York, 1997.

[3] A. Winfree. *The Geometry of Biological Time*. Springer Verlag, New York, second edition, 2001.

[4] K. Serkh and D. B. Forger. Optimal schedules of light exposure for rapidly correcting circadian misalignment. *PLoS Computational Biology*, 10(4):e1003523, 2014.

[5] B. Kralemann, M. Frühwirth, A. Pikovsky, M. Rosenblum, T. Kenner, J. Schaefer, and M. Moser. *In vivo* cardiac phase response curve elucidates human respiratory heart rate variability. *Nature Communications*, 4:2418, 2013.

[6] M. Courtemanche, L. Glass, and J. P. Keener. Instabilities of a propagating pulse in a ring of excitable media. *Physical Review Letters*, 70(14):2182, 1993.

[7] G. B. Ermentrout and D. H. Terman. *Mathematical Foundations of Neuroscience*, volume 35. Springer, New York, 2010.

[8] Y. Kuramoto. *Chemical Oscillations, Waves, and Turbulence*. Springer-Verlag, Berlin, 1984.

[9] J. Guckenheimer. Isochrons and phaseless sets. *Journal of Mathematical Biology*, 1(3):259–273, 1975.

[10] D. Jordan and P. Smith. *Nonlinear Ordinary Differential Equations: An Introduction for Scientists and Engineers*, volume 10. Oxford University Press, Oxford, 2007.

[11] K. C. A. Wedgwood, K. K. Lin, R. Thul, and S. Coombes. Phase-amplitude descriptions of neural oscillator models. *The Journal of Mathematical Neuroscience*, 3(1):2, 2013.

[12] B. Letson and J. E. Rubin. A new frame for an old (phase) portrait: Finding rivers and other flow features in the plane. *SIAM Journal on Applied Dynamical Systems*, 17(4):2414–2445, 2018.

[13] J. Cui, C. C. Canavier, and R. J. Butera. Functional phase response curves: A method for understanding synchronization of adapting neurons. *Journal of Neurophysiology*, 102(1):387–398, 2009.

[14] J. Foss and J. Milton. Multistability in recurrent neural loops arising from delay. *Journal of Neurophysiology*, 84(2):975–985, 2000.

[15] S. A. Oprisan, A. A. Prinz, and C. C. Canavier. Phase resetting and phase locking in hybrid circuits of one model and one biological neuron. *Biophysical Journal*, 87(4):2283–2298, 2004.

[16] O. Castejón, A. Guillamon, and G. Huguet. Phase-amplitude response functions for transient-state stimuli. *J. Math. Neurosci*, 3:13, 2013.

[17] D. Wilson and J. Moehlis. Isostable reduction of periodic orbits. *Physical Review E*, 94(5):052213, 2016.

[18] S. Shirasaka, W. Kurebayashi, and H. Nakao. Phase-amplitude reduction of transient dynamics far from attractors for limit-cycling systems. *Chaos: An Interdisciplinary Journal of Nonlinear Science*, 27(2):023119, 2017.

[19] D. Wilson and B. Ermentrout. Greater accuracy and broadened applicability of phase reduction using isostable coordinates. *Journal of Mathematical Biology*, 76(1-2):37–66, 2018.

[20] D. Wilson and B. Ermentrout. Augmented phase reduction of (not so) weakly perturbed coupled oscillators. To Appear in *SIAM Review*.

[21] J.H. Schleimer. *Spike statistics and coding properties of phase models*. PhD thesis, Humboldt-Universitat zu Berlin, Mathematisch-Naturwissenschaftliche Fakultat I, 2013.

[22] J. H. Schleimer and S. Schreiber. Phase-response curves of ion channel gating kinetics. *Mathematical Methods in the Applied Sciences*, 41(18):8844–8858, 2018.

[23] R. P. Boland, T. Galla, and A. J. McKane. Limit cycles, complex Floquet multipliers, and intrinsic noise.

Physical Review E, 79(5):051131, 2009.

[24] D. B. Forger, M. E. Jewett, and R. E. Kronauer. A simpler model of the human circadian pacemaker. *Journal of Biological Rhythms*, 14(6):533–538, 1999.

[25] S. H. Strogatz. *Nonlinear Dynamics and Chaos: with Applications to Physics, Biology, Chemistry, and Engineering*. Addison-Wesley, 1994.

[26] A. Bueno-Orovio, E. M. Cherry, and F. H. Fenton. Minimal model for human ventricular action potentials in tissue. *Journal of Theoretical Biology*, 253(3):544–560, 2008.

[27] F. Fenton and A. Karma. Vortex dynamics in three-dimensional continuous myocardium with fiber rotation: Filament instability and fibrillation. *Chaos*, 8(1):20–47, 1998.

[28] R. E. Kronauer, D. B. Forger, and M. E. Jewett. Quantifying human circadian pacemaker response to brief, extended, and repeated light stimuli over the phototopic range. *Journal of Biological Rhythms*, 14(6):501–516, 1999.

[29] D. B. Forger and C. S. Peskin. A detailed predictive model of the mammalian circadian clock. *Proceedings of the National Academy of Sciences*, 100(25):14806–14811, 2003.

[30] S. Coombes, R. Thul, and K. C. A. Wedgwood. Nonsmooth dynamics in spiking neuron models. *Physica D: Nonlinear Phenomena*, 241(22):2042–2057, 2012.

[31] M. di Bernardo, C. Budd, A. R. Champneys, and P. Kowalczyk. *Piecewise-smooth dynamical systems: theory and applications*, volume 163. Springer, London, 2008.

[32] C. A. Klausmeier. Floquet theory: a useful tool for understanding nonequilibrium dynamics. *Theoretical Ecology*, 1(3):153–161, 2008.

[33] E. Brown, J. Moehlis, and P. Holmes. On the phase reduction and response dynamics of neural oscillator populations. *Neural Computation*, 16(4):673–715, 2004.

[34] Y. Park, K. M. Shaw, H. J. Chiel, and P. J. Thomas. The infinitesimal phase response curves of oscillators in piecewise smooth dynamical systems. *European Journal of Applied Mathematics*, pages 1–36, 2018.

[35] T. R. Shannon, F. Wang, J. Puglisi, C. Weber, and D. M. Bers. A mathematical treatment of integrated Ca dynamics within the ventricular myocyte. *Biophysical Journal*, 87(5):3351–3371, 2004.

[36] V. Iyer, R. Mazhari, and R. L. Winslow. A computational model of the human left-ventricular epicardial myocyte. *Biophysical Journal*, 87(3):1507–1525, 2004.

[37] K. H. W. J. ten Tusscher, D. Noble, P. J. Noble, and A. V. Panfilov. A model for human ventricular tissue. *American Journal of Physiology-Heart and Circulatory Physiology*, 286(4):H1573–H1589, 2004.

[38] J. J. Fox, R. Bodenschatz, and T. G. Gilmour Jr. Period-doubling instability and memory in cardiac tissue. *Physical Review Letters*, 89(13):138101, 2002.

[39] E. M. Cherry, F. H. Fenton, and R. F. Gilmour Jr. Mechanisms of ventricular arrhythmias: a dynamical systems-based perspective. *American Journal of Physiology-Heart and Circulatory Physiology*, 302(12):H2451, 2012.

[40] E. J. Pruvot, R. P. Katra, D. S. Rosenbaum, and K. R. Laurita. Role of calcium cycling versus restitution in the mechanism of repolarization alternans. *Circulation Research*, 94(8):1083–1090, 2004.

[41] S. M. Narayan. T-wave alternans and the susceptibility to ventricular arrhythmias. *Journal of the American College of Cardiology*, 47(2):269–281, 2006.

[42] J. M. Pastore, S. D. Girouard, K. R. Laurita, F. G. Akar, and D. S. Rosenbaum. Mechanism linking T-wave alternans to the genesis of cardiac fibrillation. *Circulation*, 99(10):1385–1394, 1999.

[43] D. J. Christini, M. L. Riccio, C. A. Culianu, J. J. Fox, A. Karma, and R. F. Gilmour Jr. Control of electrical alternans in canine cardiac Purkinje fibers. *Physical Review Letters*, 96(10):104101, 2006.

[44] P. N. Jordan and D. J. Christini. Adaptive diastolic interval control of cardiac action potential duration alternans. *Journal of Cardiovascular Electrophysiology*, 15(10):1177–1185, 2004.

[45] M. Li and N. F. Otani. Controlling alternans in cardiac cells. *Annals of Biomedical Engineering*, 32(6):784–792, 2004.

[46] D. Wilson and J. Moehlis. Spatiotemporal control to eliminate cardiac alternans using isostable reduction. *Physica D: Nonlinear Phenomena*, 342:32–44, 2017.

[47] A. Garzón, R. O. Grigoriev, and F. H. Fenton. Model-based control of cardiac alternans in Purkinje fibers. *Physical Review E*, 84(4):041927, 2011.

[48] Y. Prudat, R. V. Madhvani, M. Angelini, N. P. Borgstom, A. Garfinkel, H. S. Karagueuzian, J. N. Weiss, E. Lange, R. Olcese, and J. P. Kucera. Stochastic pacing reveals the propensity to cardiac action potential alternans and uncovers its underlying dynamics. *The Journal of Physiology*, 594(9):2537–2553, 2016.

[49] E. M. Cherry and F. H. Fenton. Suppression of alternans and conduction blocks despite steep APD restitution: electrotonic, memory, and conduction velocity restitution effects. *American Journal of Physiology-Heart and Circulatory Physiology*, 55(6):H2332–H2341, 2004.

[50] E. G. Tolkacheva, D. G. Schaeffer, D. J. Gauthier, and W. Krassowska. Condition for alternans and stability of the 1:1 response pattern in a memory model of paced cardiac dynamics. *Physical Review E*, 67(3):031904, 2003.

[51] S. Wiggins. *Introduction to Applied Nonlinear Dynamical Systems and Chaos*, volume 2. Springer, 2003.

[52] C. Grebogi, E. Ott, and J. A. Yorke. Basin boundary metamorphoses: changes in accessible boundary orbits.

Nuclear Physics B-Proceedings Supplements, 2:281–300, 1987.

[53] D. Kirk. *Optimal Control Theory*. Dover Publications, New York, 1998.

[54] G. B. Ermentrout, B. Beverlin II, T. Troyer, and T. I. Netoff. The variance of phase-resetting curves. *Journal of Computational Neuroscience*, 31(2):185–197, 2011.

[55] C. W. Gardiner. *Handbook of Stochastic Methods: for Physics, Chemistry and the Natural Sciences*. Springer, Berlin, 2004.

[56] A. Mauroy and I. Mezic. Global computation of phase-amplitude reduction for limit-cycle dynamics. *arXiv preprint 1803.07379*, 2018.

[57] A. Guillamon and G. Huguet. A computational and geometric approach to phase resetting curves and surfaces. *SIAM Journal on Applied Dynamical Systems*, 8(3):1005–1042, 2009.

[58] M. Detrixhe, M. Doubeck, J. Moehlis, and F. Gibou. A fast Eulerian approach for computation of global isochrons in high dimensions. *SIAM Journal on Applied Dynamical Systems*, 15(3):1501–1527, 2016.